Title

Volcano infrasound and the International Monitoring System

ISBN

978-3-319-75140-5

Authors

Matoza, Robin Samuel

Fee, D.

Green, D.

et al.

Publication Date

2019

Peer reviewed

Chapter 33
Volcano Infrasound and the International Monitoring System

Robin Matoza, David Fee, David Green and Pierrick Mialle

Abstract Volcanoes generate a wide variety of low-frequency (~0.01–20 Hz) acoustic signals, and infrasound technology is part of an expanding suite of geophysical tools available to characterize, understand, and monitor volcanic processes. We review recent advances in the field of volcano acoustics with an emphasis on scientific and potential civil application gains from the International Monitoring System (IMS) infrasound network. Energetic infrasound from explosive volcanism can propagate hundreds to thousands of kilometers in atmospheric waveguides and large explosive eruptions (which represent significant societal and economic hazards) are routinely recorded by the IMS infrasound network. Significant progress in understanding volcano infrasound has been made through dedicated local deployments (within <15 km of the source) in tandem with other observation systems. This research has identified diverse source mechanisms of volcanically generated infrasound, and elucidated the influence of near-source topography and local atmospheric conditions on acoustic propagation and recordings. Similarly, advances are being achieved in inferring volcanic source processes from signals recorded at the longer ranges typically associated with IMS detections. However, practical challenges remain in the optimization of remote volcano infrasound signal detection, discrimination, association, and location. Many of these challenges are the result of strong signal variability associated with long-range

R. Matoza (✉)
Department of Earth Science and Earth Research Institute,
University of California, Santa Barbara, CA, USA
e-mail: matoza@geol.ucsb.edu

D. Fee
Wilson Alaska Technical Center and Alaska Volcano Observatory,
Geophysical Institute, University of Alaska Fairbanks, Fairbanks, AK, USA

D. Green
AWE Blacknest, Brimpton, UK

P. Mialle
CTBTO, Vienna, Austria

A. Le Pichon et al. (eds.), *Infrasound Monitoring for Atmospheric Studies*,
https://doi.org/10.1007/978-3-319-75140-5_33

acoustic propagation through the temporally and spatially varying atmosphere. We review the state of knowledge on infrasound generation by explosive volcanism, and assess progress toward the development of infrasonic eruption early warning and notification systems at regional and global scales.

33.1 Volcano Acoustics in Context

Infrasound technology adds to a growing suite of geophysical tools available to characterize, understand, and monitor volcanic processes. A better understanding of volcanic eruption processes helps to mitigate the associated societal and economic hazards, which have the potential to affect more people as global population density and air traffic increase (e.g., Casadevall et al. 1994; Chester et al. 2000; Annen and Wagner 2003).

Volcanic eruptions are spectacular manifestations of the dynamic nature of our planet. As a consequence of plate tectonics and mantle convection, melt formed at depth migrates to the surface through a complicated network of cracks, fissures, and conduits to form surface volcanism. On longer timescales, magma migration and storage may be expressed in ground deformation recorded with strain- and tilt-meters, Global Positioning System receivers, and satellite radar interferometry (e.g., Dzurisin 2006; Segall 2010). Volcano seismology and volcano acoustics are two

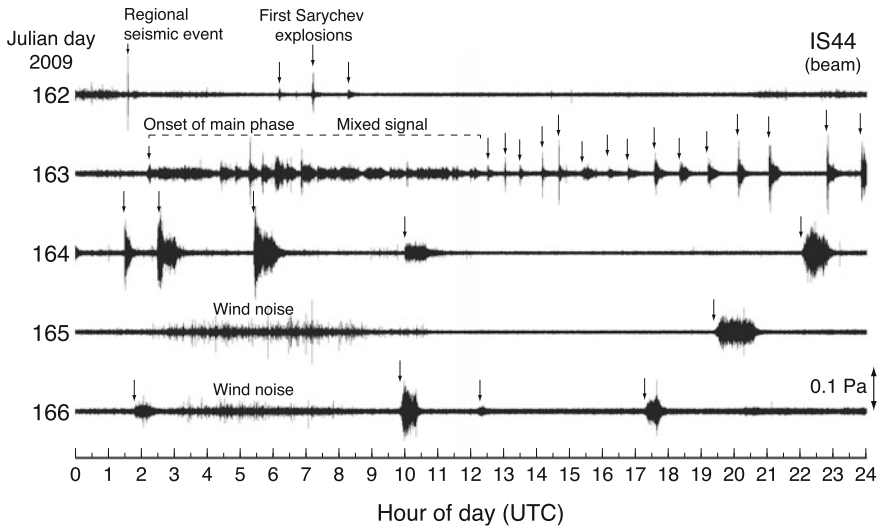

Fig. 33.1 Infrasonic waveforms recorded at IS44 (Kamchatka) for the June 2009 eruption of Sarychev Peak, Kuriles (5 days: 11–15 June 2009, or Julian days 162–166 2009). Each waveform shows one full day of data. Infrasound array data have been beamformed (waveforms aligned and stacked for azimuth of Sarychev Peak and acoustic velocity) using a time-delay beamformer and filtered 0.5–5 Hz. (Figure reproduced from Matoza et al. 2011a)

complementary methods for understanding more rapid phenomena associated with fluid storage, transport, and eruption from the subsurface to the atmosphere. Recording signals in the same frequency range (hundreds of seconds to tens of Hz), seismic and acoustic data together represent a more complete recording of the elastic wavefield radiated by volcanoes. Seismic waves are produced by subsurface magmatic, hydrothermal, and faulting processes occurring within and around volcanoes from mantle depths to the surface (e.g., Chouet and Matoza 2013). Acoustic waves are produced by shallow subsurface and subaerial processes, including explosive eruptions, shallow degassing, surface flow, and mass wasting. Seismic and acoustic signals have been observed for decades at some persistently erupting volcanoes, with temporal evolution in these signals containing rich information on

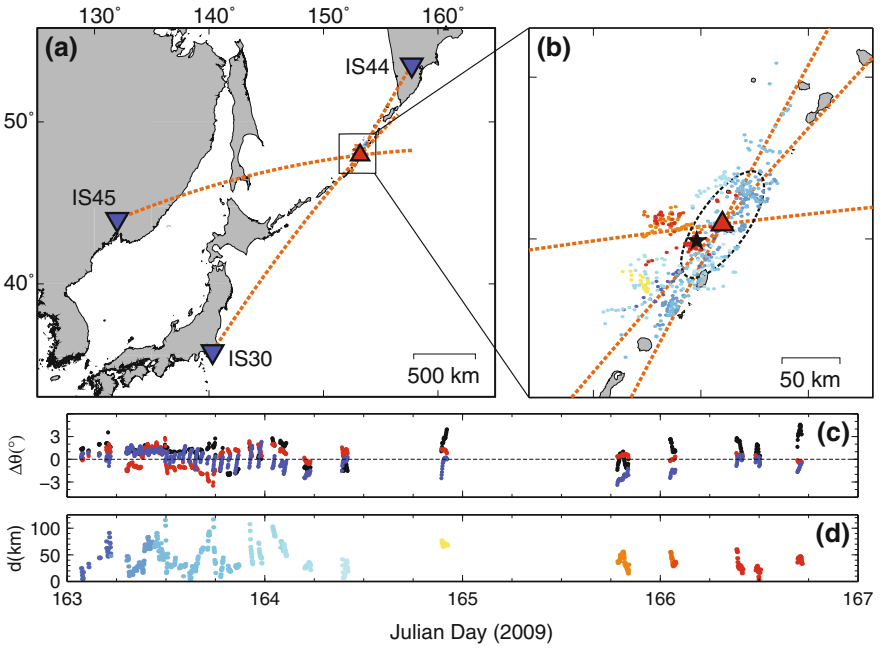

Fig. 33.2 Infrasonic source location for the June 2009 eruption of Sarychev Peak (large red triangle) via back azimuth cross-bearings using the closest three IMS arrays: IS44, IS45, and IS30 (inverted blue triangles). Seven arrays (not shown) recorded infrasound from this event out to 6,400 km from the source. **a**, **b** Source location is performed on a running median of the observed signals and a back azimuth correction is applied using 3D ray-tracing and ECMWF, HWM07, and MSIS90 atmospheric specifications (Matoza et al. 2011a). The source location solutions (dots) are colored as a function of time corresponding to (**d**). The mean source centroid is shown as a black star. Dashed ellipse shows 90% confidence for source location assuming azimuth errors normally distributed around true with a standard deviation of 3°. Dashed lines are the true great-circle path azimuths from each station to Sarychev Peak. **c** Running median signal azimuth deviation at the three stations (black: IS44, red: IS45, blue: IS30). Times are corrected for a constant celerity of 0.33 km/s. **d** Source location error: distance [km] between true Sarychev Peak location and the obtained infrasonic source locations. (Figure modified from Matoza et al. 2011a)

the multi-year eruption dynamics (e.g., Ripepe et al. 2007; Iguchi 2013; Matoza et al. 2013a).

Explosive eruptions are seismo-acoustic phenomena, generating large-amplitude acoustic waves as well as seismic waves. Precursory and co-eruptive seismicity includes individual volcano-tectonic (VT) earthquakes, long-period (LP) (0.5–5 Hz) events, and various types of volcanic tremor (Chouet and Matoza 2013). The typical seismic expression of a sustained explosive eruption, a broadband signal (~0.1–20 Hz) known as *eruption tremor* (McNutt 2000; McNutt and Nishimura 2008), usually has a limited propagation distance. The maximum observation range for eruption tremor is typically a few tens of kilometers, or up to a few hundred kilometers for larger eruptions (e.g., Prejean and Brodsky 2011). In contrast, similar-sized explosive eruptions produce powerful broadband (~0.01–20 Hz) infrasound signals (Fig. 33.1) that can be ducted efficiently over long ranges (thousands of kilometers) in atmospheric waveguides. These infrasound signals are now routinely detected on sparse ground-based infrasound networks such as the International Monitoring System (IMS) (e.g., Fee et al. 2010a, b; Matoza et al. 2011a, b; Dabrowa et al. 2011; Green et al. 2012; Fee et al. 2013a, b). In remote volcanic regions, infrasound is sometimes the only ground-based technology to record an explosive eruption and can therefore provide vital information to complement satellite data and constrain ash-release parameters for aviation safety (Figs. 33.2 and 33.3; e.g., Matoza et al. 2011a). At seismically instrumented

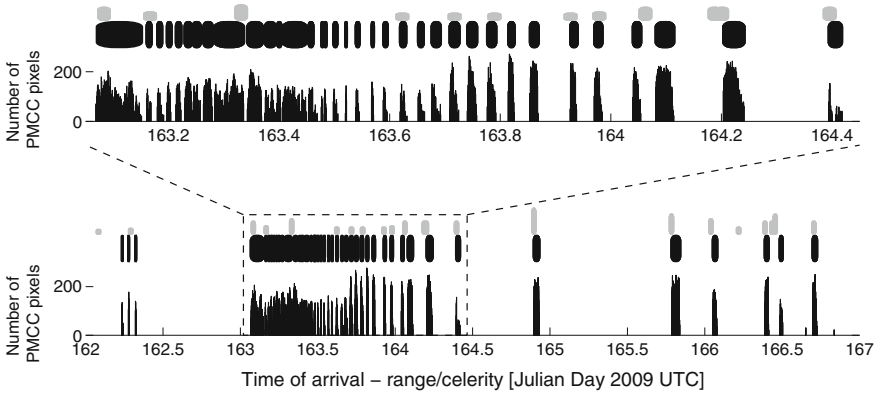

Fig. 33.3 Chronology of coherent infrasonic signal at IS44 from the June 2009 eruption of Sarychev Peak compared to the eruption chronology inferred from satellite data by the Sakhalin Volcanic Eruptions Response Team (SVERT). Lower plot: number of Progressive Multi-Channel Correlation (PMCC) (Cansi 1995) detections per minute at IS44 originating from the direction of Sarychev Peak. Time of arrivals are corrected back to an inferred origin time at Sarychev assuming a celerity of 0.33 km/s. Black horizontal bars above plot represent beginning and end times of coherent signal packets. Gray bars represent explosion onset times ±15 min inferred from satellite data by SVERT. Vertical extent of each gray bar is scaled relative to the maximum plume altitude inferred by SVERT. Upper plot: an expanded view of lower plot between Julian days 163–164.5 2009. (Figure reproduced from Matoza et al. 2011a)

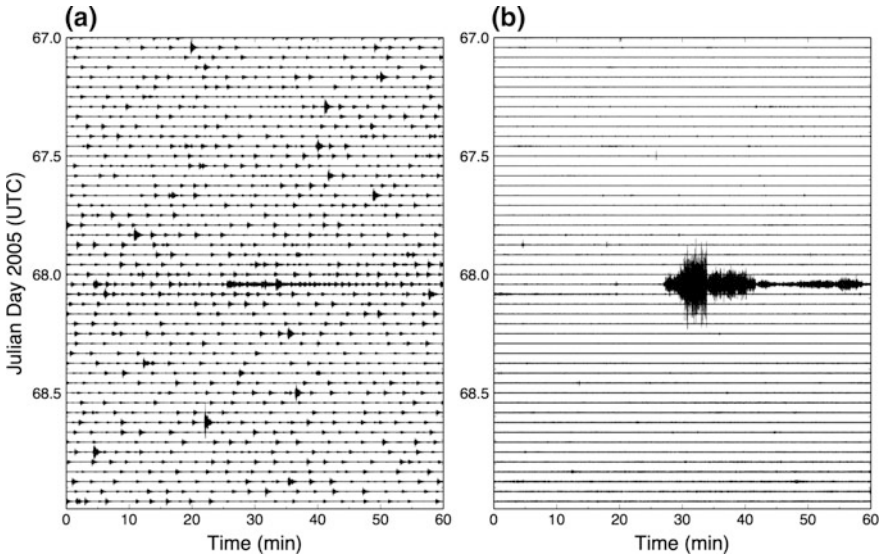

Fig. 33.4 **a** Seismic vertical component velocity and **b** infrasonic pressure recordings of the 8 March 2005 phreatic (steam-driven) explosion of Mount St. Helens, Washington, USA. The broadband seismometer was collocated with the central element of a 4-element infrasound array CDWR in a quiet forest site ~13.4 km from the source (Matoza et al. 2007). In each case, we show data from ±1 day spanning the event at 9 March 2005 ~01:26:17 UTC (day 68). The seismic tremor accompanying the phreatic explosion has a similar amplitude to seismicity before and after. A large unambiguous infrasound signal delineates the explosive eruption timing (Matoza et al. 2007)

volcanoes, infrasound data reduce ambiguity in explosion detection by clearly delineating the timing and duration of explosive eruption (Fig. 33.4); this is particularly useful when the volcano is visually obscured by cloud cover (Matoza et al. 2007). Because infrasound is radiated directly from explosive eruption processes in the atmosphere, the signals contain important constraints for physical volcanology (e.g., Cerminara et al. 2016), including estimates of the time-history of volume flux and potentially mass flux (e.g., Johnson et al. 2008a; Kim et al. 2015).

Several review papers and book chapters already exist, offering various perspectives on the field of volcano infrasound (e.g., Johnson and Ripepe 2011; Garces et al. 2013; Fee and Matoza 2013; McNutt et al. 2015). The present chapter reviews the history, development, and recent advances in the field of volcano acoustics with an emphasis on science and potential civil application gains from the IMS network.

33.2 History of Volcano Infrasound

Volcanoes generate a wide variety of acoustic signals within the infrasonic frequency band (~0.01–20 Hz) and explosive volcanic eruptions are among the most powerful sources of infrasound observed on Earth. More generally, volcano infrasound is part of a broad spectrum of atmospheric waves produced by volcanic activity that includes gravity waves, acoustic-gravity waves, infrasound, and audible acoustic signals (Gossard and Hooke 1975).

33.2.1 Barograph Studies and Infrasound Microphone Arrays (<1 Hz)

In 1883, over 50 weather barometers around the world recorded long-period pressure disturbances from the cataclysmic, Volcanic Explosivity Index[1] (VEI) 6, August 27 eruption of Krakatau Volcano, Indonesia (Fig. 33.5) (Scott 1884; Strachey 1884, 1888; Verbeek 1884). A Royal Society of London report compiled the barometric observations and reports of sounds heard (Strachey 1888). Cannon-like sounds were audible as far away as ~5,000 km. This phenomenon of long-distance audible sound from Krakatau is now explained by nonlinear wave steepening and reshocking rather than unattenuated audible frequencies from near the source (Lonzaga et al. 2015). The long-period pressure wave, recorded as barometric pulses, propagated as many as seven times around the globe (Strachey 1888). It took roughly 1.5 days to make each complete lap, with an average propagation speed of 300–325 m/s; the dominant periods at long range were ~100–200 min (Fig. 33.5) (Gabrielson 2010). These remarkable observations stimulated the development of theory to explain these acoustic-gravity waves, to understand the effects of gravity, buoyancy, and atmospheric structure on the acoustic propagation from such an immense source (e.g., LeConte 1884; Lamb 1911; Taylor 1929, 1936; Pekeris 1939; Pierce 1963; Press and Harkrider 1962, 1966; Harkrider 1964; Harkrider and Press 1967; see Gabrielson 2010 for a review).

In a pioneering study of earthquakes and airborne explosions ("detonations") at Mount Asama, Japan, Omori (1912) used seismometers and barometers to discriminate between seismic signals associated with explosions and non-explosion earthquakes. Many of the explosion events were audible in settlements at distances of ~200–300 km (Fig. 33.6), and some were powerful enough to knock out doors and windows. Omori used this information to map the sound propagation and acoustic shadow zones, and considered the effects of wind and topography on the

[1]VEI is a semi-quantitative measure of the magnitude or size of explosive eruptions based on factors such as the erupted ejecta volume, column height, and explosive eruption duration (Newhall and Self 1962). The VEI estimates given throughout the text are from the Smithsonian database of Siebert and Simkin (2002).

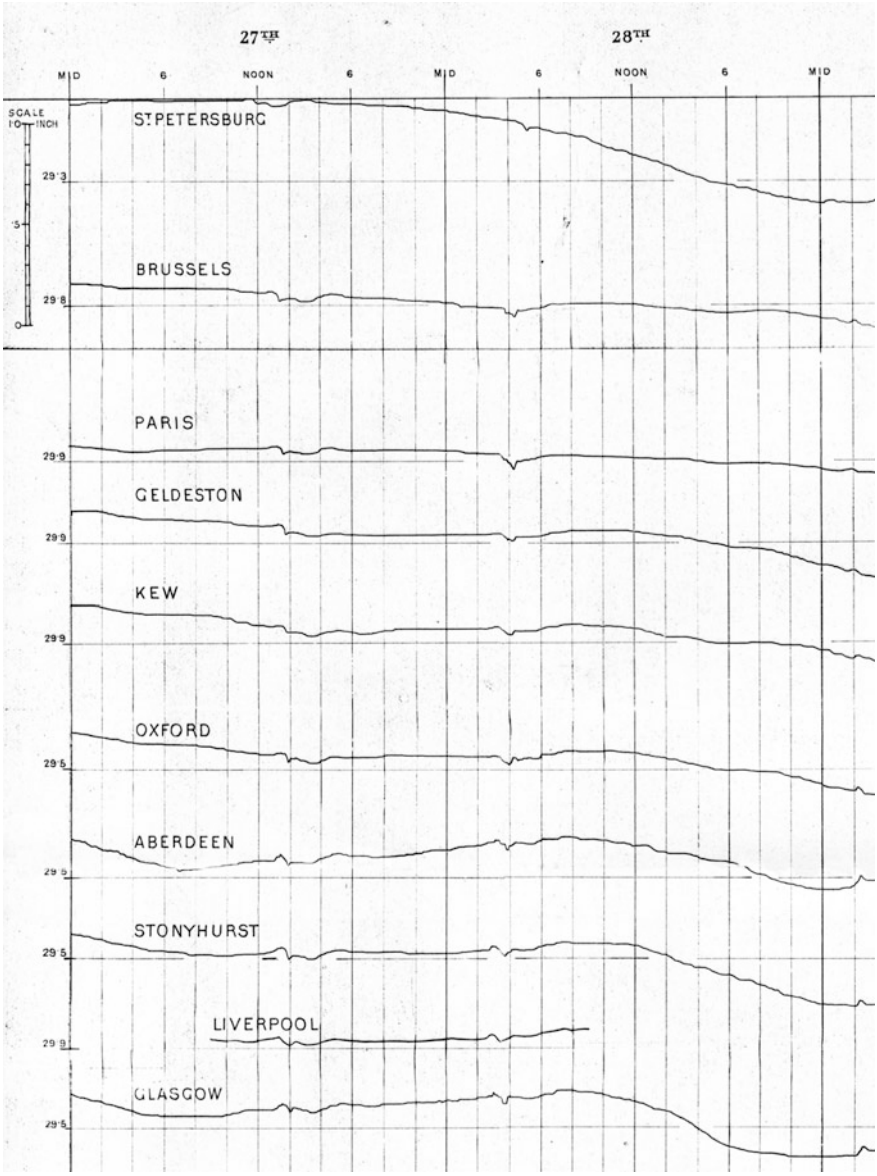

Fig. 33.5 Barograms from the 27 August 1883 eruption of Krakatau showing the first two wave passages. The traces are shown on a common scale and times are in UTC. The horizontal divisions are 2 h and 1 inch of mercury is ~3,386 Pa. (Figure reproduced and modified from Scott 1884)

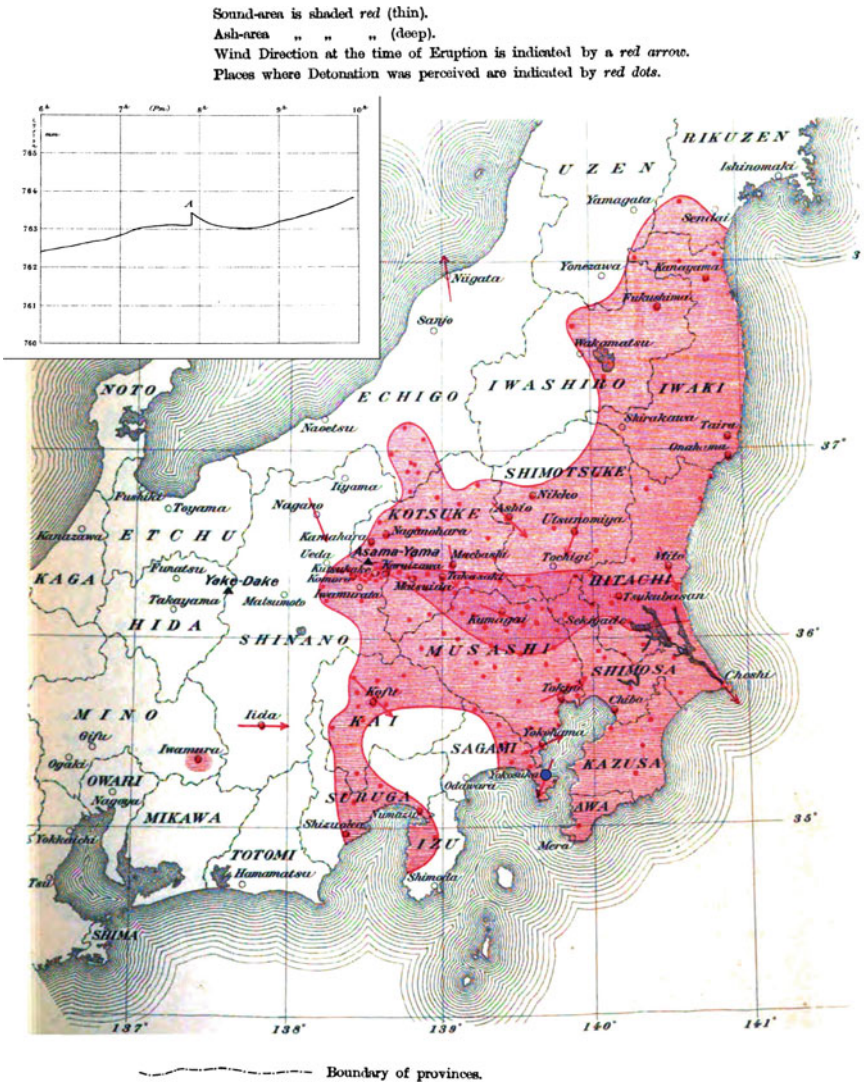

Fig. 33.6 Zone of audibility of "detonation" sound from a 7 December 1909 explosion of Asamayama, Japan (Omori 1912). The light red region is the audibility region, while the dark red region is the ash fallout region. Inset shows barogram at the Meteorological Observatory of Yokosuka (blue circle in map) for the same eruption (*A* marks signal onset). (Figures reproduced and modified from Omori 1912)

acoustic signals (Fig. 33.6). It is noteworthy that this classic early paper in volcano seismology gave equal emphasis to seismic and acoustic wavefields.

The use of weather barometers and infrasonic microphone arrays to study low-frequency (<1 Hz) atmospheric pressure waves from volcanic explosions at regional to global ranges (tens to thousands of kilometers) continued throughout the

twentieth century, e.g., Mount Pelee, Martinique 1902 (Tempest and Flett 1903); Bezymianny, Russia 1956 (Gorshkov 1960); Mount St. Helens, USA 1980 (Reed 1987; Delclos et al. 1990); El Chichon, Mexico 1982 (Mauk 1983); Mount Tokachi, Japan 1988; Sakurajima, Japan 1989; Mount Pinatubo, Philippines 1991; and Ruapehu, New Zealand 1995 (Morrissey and Chouet 1997). Goerke et al. (1965), Wilson et al. (1966), and Wilson and Forbes (1969) provided some of the first infrasonic microphone array observations of volcanoes in the low infrasound band (0.01–0.1 Hz). The 1963 eruption of Mount Agung, Bali was recorded 14,700 km away in Boulder, Colorado (Goerke et al. 1965); and the 1967 eruptions of Redoubt and Trident Volcanoes, Alaska, were recorded in Fairbanks, Alaska (Wilson et al. 1966; Wilson and Forbes 1969). The main emphasis of these studies was the atmospheric propagation of the signals.

The 18 May 1980 VEI 5 eruption of Mount St. Helens was particularly well recorded and studied. Similar to the work by Omori (1912) (Fig. 33.6), audibility zones were mapped by Fairfield (1980) as far as 700 km from the source. Weather barograph stations across the Pacific Northwest (out to ~400 km) recorded the event (Bannister 1984; Reed 1987). Pressure waves were recorded worldwide over 7,000 km from the source on microbarograph and infrasonic microphone arrays, and have been modeled as a combination of Lamb and acoustic-gravity modes (Bolt and Tanimoto 1981; Donn and Balachandran 1981; Bath 1982; Liu et al. 1982; Delclos et al. 1990). Using pressure-distance empirical scaling relations (Glasstone 1977), Reed (1987) estimated the equivalent nuclear yield of the main blast at a few megatons. Barograph signals with period ~300 s and observed peaks in seismic Rayleigh wave spectra were attributed to atmospheric oscillations (gravity mode and acoustic normal modes) excited by the eruption (Kanamori et al. 1994; Watada and Kanamori 2010). Infrasound air–ground-coupled waves were also recorded across a seismic network in Washington State (Johnson and Malone 2007).

Infrasonic microphone arrays were installed at Kariya, Japan (Tahira 1982) and Windless Bight, Antarctica, 26 km from Mount Erebus (Dibble et al. 1984). Although limited to the band 0.1–1 Hz, the Kariya array routinely detected explosions from Sakurajima Volcano at a range of 710 km and also recorded the 1991 Pinatubo, Philippines eruption at a range of 2,770 km. These data were used to infer the eruptive time-history when visual or instrumental observations close to the volcano were impossible (Tahira et al. 1996).

33.2.2 Audible Sound Microphone Recordings (>20 Hz)

Frank Perret made probably the first recordings of audible sounds (>20 Hz) from volcanoes using moving-coil microphones at Vesuvius Volcano, Italy in 1906, eventually recording signals at Etna and Stromboli Volcanoes, Italy; Kilauea Volcano, Hawaii; Sakurajima Volcano, Japan; Mt. Pelee Volcano, Martinique; and Soufriere Hills Volcano, Montserrat (Perret 1950). The NHK Broadcasting Bureau of Japan apparently made the first tape recordings of volcanic sounds (Snodgrass and

Richards 1956). In 1952, a program of volcanic acoustics was initiated by James Snodgrass at the Scripps Institution of Oceanography, leading to a decade's worth of underwater and airborne acoustic recordings of volcanic sounds (Richards 1963). The paper by Richards (1963) summarizes the observations, relating the various sounds to different idealized styles of volcanic activity; however, the sonobuoy-based recording systems had a poor frequency response below 50 Hz. A pioneering study of acoustic signals (>20 Hz) by Woulff and McGetchin (1976) represents the first attempt at a quantitative link between acoustic radiation and fluid mechanics at volcanoes using equivalent source theory (Sect. 33.6.1). Naturally, audible sound from volcanoes is readily recordable close to the source (e.g., Lorenz et al. 2015).

33.2.3 Volcano Infrasound (0.01–20 Hz)

As with volcano seismology, the long-period (LP) band (0.5–5 Hz) tends to be an especially rich band for volcano-acoustic sources. Progress in the field of volcano acoustics was therefore modest until microphones targeting these frequencies were deployed near active volcanoes. *Near-infrasound* (1–20 Hz) from volcanoes is documented from the 1980s (e.g., Dibble et al. 1984; Firstov and Kravchenko 1996). Iguchi and Ishihara (1990) and Yamasato (1997) installed infrasonic microphones at distances of 2–5 km from Sakurajima, Suwanosejima, and Unzen Volcanoes in Japan, recording numerous explosions, pyroclastic flows (Yamasato 1997), harmonic infrasonic tremor (Sakai et al. 1996), and impulsive signals associated with LP events (Iguchi and Ishihara 1990; Yamasato 1998). Acoustic studies began at Stromboli Volcano in the early 1990s (Braun and Ripepe 1993; Vergniolle and Brandeis 1994; Buckingham and Garces 1996). Since then, it has become increasingly clear that a great variety of volcanic processes produce a diverse spectrum of infrasound across the 0.01–20 Hz frequency range (e.g., Fee and Matoza 2013).

33.2.4 The IMS Infrasound Network

In 1996 the Comprehensive Nuclear-Test-Ban Treaty (CTBT) was opened for signature. The treaty called for a verification regime to be established, of which the IMS is one element. The IMS infrasound network (Fig. 33.7) is designed to detect atmospheric explosions anywhere on the planet, with early studies citing a nominal threshold yield equivalent to 1 kiloton of TNT (Christie and Campus 2010). However, simulations show that long-range stratospheric ducting of infrasound significantly enhances the detection capability, with explosions of a couple hundred tons TNT equivalent being detectable globally at two or more stations on the complete network (Le Pichon et al. 2009; Green and Bowers 2010). Data holdings from the IMS infrasound network go back to about 2001 and as of 2015 the IMS has 49 certified stations out of a planned total of 60. Each infrasound station

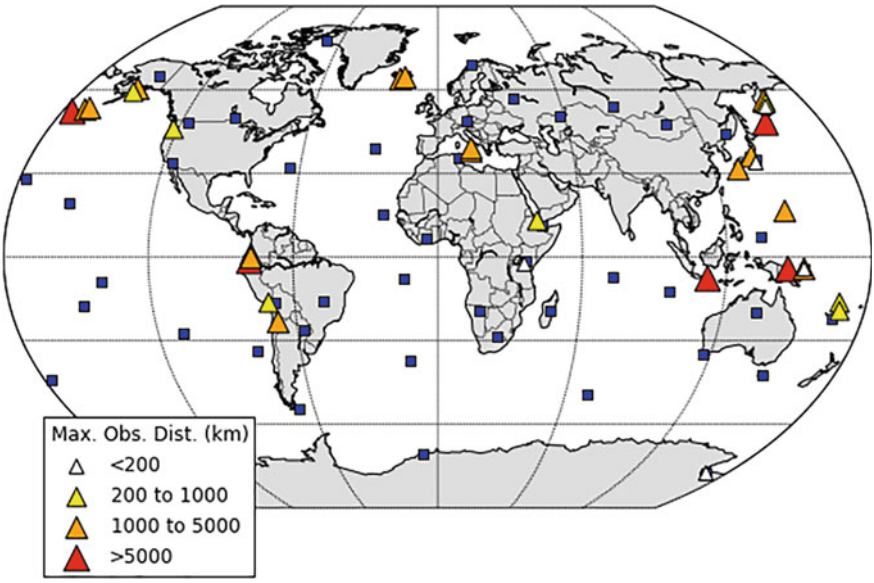

Fig. 33.7 The IMS infrasound array network as of 2015 (blue squares), and 43 volcanoes for which infrasound signals have been reported at an IMS station in the peer-reviewed literature (triangles). The color of the triangle refers to the furthest signal detection distance for all reported eruptions at the volcano. Multiple explosive events have been recorded from many of these volcanoes since the inception of the IMS. (Figure adapted and updated from Dabrowa et al. 2011)

consists of an array of at least four infrasonic sensors sampling atmospheric pressure at 20 Hz with a flat response compliant with IMS minimum requirements from 0.02 to 4 Hz and a sensitivity of about 0.1 mPa per count. The average station spacing for the complete network will be about 2,000 km (Christie and Campus 2010). The construction of the IMS has led to rapid advances in infrasound technology, and improved our ability to use infrasound to understand and monitor volcanic processes (Fig. 33.7). Two of the next stations planned for construction are: IS01 (Bariloche, west of Argentina close to the Andes) and IS20 (Galapagos, Ecuador) that will extend and improve IMS capabilities to monitor volcanic eruptions in the Latin America region.

33.3 Volcano-Acoustic Observation Systems

Volcanic infrasound sensor acquisition geometries include networks of individual infrasound sensors (e.g., Braun and Ripepe 1993; Garces et al. 1999; Hagerty et al. 2000; Johnson 2003; Moran et al. 2008; Lees et al. 2008; Cannata et al. 2009; Fee et al. 2014) and infrasound arrays, including networks of infrasound arrays such as the IMS infrasound network (e.g., Ripepe and Marchetti 2002; Guilbert et al. 2005;

Matoza et al. 2007; Taisne et al. 2019; Garces et al. 2008; Matoza et al. 2011b; De Angelis et al. 2012; Taisne et al. 2012, 2019; Tailpied et al. 2013). Where extensive infrasound sensor observations are limited, infrasound waves may still be tracked using collocated seismic and infrasonic sensor pairs (e.g., Ichihara et al. 2012; Matoza and Fee 2014; Nishida and Ichihara 2016) or solely using air–ground-coupled waves on seismic networks (e.g., Cochran and Shearer 2006; Johnson and Malone 2007; Fee et al. 2016). Networks of single infrasound sensors are often adequate for local deployments (nominally defined as <15 km from the source; Fee and Matoza 2013) around volcanoes that produce high-amplitude transient signals (e.g., volcanic "explosions"), whose relative arrival times can be tracked across the network (e.g., Johnson 2003; Fee et al. 2014). However, low-amplitude transients (e.g., Matoza et al. 2009a) or tremor signals (e.g., associated with sustained degassing or lahars) may require infrasound arrays for unambiguous detection and discrimination from background noise even at local distances (Garces et al. 2003; Matoza et al. 2007; Fee and Garces 2007; Matoza et al. 2010; Johnson and Palma 2015). Local deployments are also still subject to time-varying atmospheric propagation effects (Sect. 33.7), for which arrays provide useful additional information. At regional distances (nominally 15–250 km) and global distances (>250 km), infrasound arrays provide significant advantages for the detection and identification of remote volcanic infrasound signals within incoherent wind noise (Walker and Hedlin 2010) and coherent infrasonic clutter (Matoza et al. 2013c). Nevertheless, significant advances are being made toward using networks of single infrasound sensors or networks of seismic and infrasonic sensor pairs to identify remote volcanic infrasound at regional to global distances (e.g., Ichihara et al. 2012; Matoza and Fee 2014; Nishida and Ichihara 2016).

33.3.1 Remote Volcanic Signal Discrimination Using Arrays

Since the IMS infrasound network consists of a network of infrasound arrays, here we discuss some practical considerations for the use of IMS-style infrasound arrays for the detection of remote explosive volcanism. An example of long-range infrasonic array observations of explosive volcanism is shown in Fig. 33.8, which shows the detection of the 2010 eruption of Eyjafjallajökull, Iceland at station BKNI, UK. An initial burst of infrasound from this event was recorded from 14 to 15 April 2010, with the major long-duration infrasound recorded from April 18 to May 20, 2010 (Matoza et al. 2011b). The 2010 eruption of Eyjafjallajökull was recorded by 14 infrasound arrays at ranges between 1,745 and 3,666 km, indicating that infrasound from modest-size eruptions can propagate for thousands of kilometers in atmospheric waveguides. BKNI (4-element array) was the closest remote infrasound array to Eyjafjallajökull (range 1,745 km) considered by Matoza et al. (2011b). As shown in Fig. 33.8a, the volcano falls at a similar back azimuth to the microbarom source region at this time of year (Landès et al. 2012; see also the work

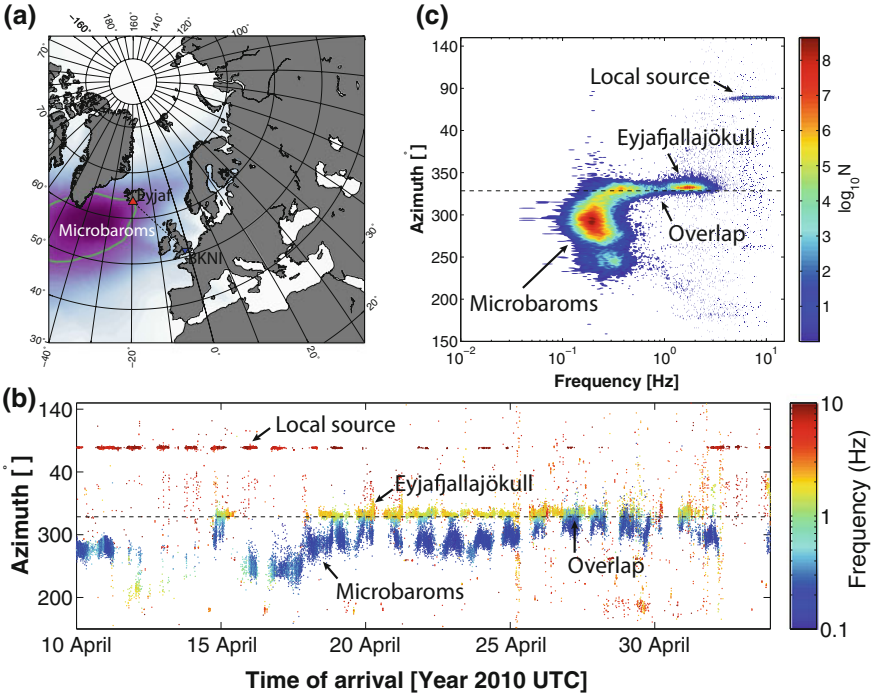

Fig. 33.8 Remote infrasonic array observations of the 2010 eruption of Eyjafjallajökull at station BKNI (Blacknest, UK; range 1,745 km, 4-element infrasound array). **a** Station BKNI (blue inverted triangle) and Eyjafjallajökull (red triangle) are shown in relation to the inferred source distribution of oceanic microbaroms in April from Landès et al. (2012). Purple grid values represent high probability of microbarom sources; the grid represents a multi-year average for 2006–2010 for the calendar month of April. **b** Log-scale PMCC processing results for the eruption onset (Matoza et al. 2011b). PMCC pixels are plotted by back azimuth and color-scaled by frequency content; the dashed line is the true back azimuth to Eyjafjallajökull (see a). An initial burst of infrasonic detections from Eyjafjallajökull (yellow dots) begins on April 14–15, is followed by repose from 15–17 April, and the onset of the main phase occurs on 18 April 2010. A higher frequency local source (red dots) and lower frequency microbarom source (dark blue dots) are also recorded by the array. **c** Frequency-azimuth space density plot of the data shown in (**b**), with the color scale representing the number of points (*N*)

by Evers and Haak 2001); the microbarom back azimuth is variable for this spatially extensive source. At times (e.g., April 15–20, 2010), the azimuths are distinct enough to allow for separation of microbarom and volcanic sources (Fig. 33.8b); however, later in the sequence the back azimuth values overlap and the microbarom interferes with the volcanic signal (Fig. 33.8b). Figure 33.8b, c reveal that each source usually occupies a distinct area of frequency-azimuth space, but occasional overlap in mean frequency and azimuth require more advanced signal detection and discrimination procedures. The example shown in Fig. 33.8 highlights how an infrasound array helps to discriminate volcanic signals of interest (in comparison to a remote single infrasonic sensor).

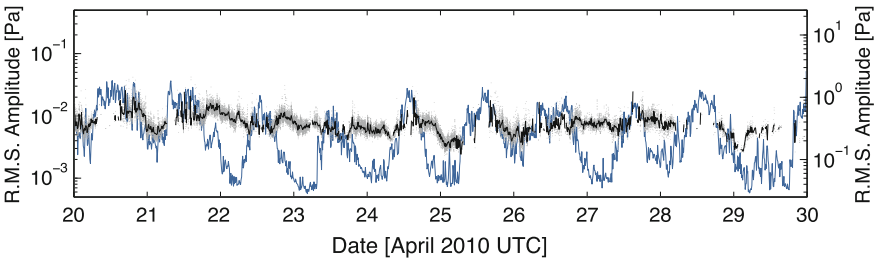

Fig. 33.9 Signal and noise amplitude variations at array BKNI, UK. PMCC detection root-mean-square (RMS) amplitudes (gray dots, left- hand scale) and their 10-minute median values (black line, left-hand scale) indicate coherent acoustic detections associated with Eyjafjallajökull. This is compared to RMS amplitude at one element in the 0.01–0.5 Hz band (blue line, right-hand scale). (Figure reproduced from Matoza et al. 2011b)

An additional feature of the BKNI recordings of the 2010 Eyjafjallajökull eruption is the diurnal variation in received signal characteristics (Fig. 33.8b), which were investigated in detail by Green et al. (2012). This is illustrated in Fig. 33.9, which shows the diurnal variability of signal reception compared to root-mean-square (RMS) amplitude at low frequencies (0.01–0.5 Hz), a useful proxy for wind noise (Fee and Garces 2007). Such observations are important for the remote identification of volcanic infrasound and again are facilitated by the use of arrays rather than single infrasound sensors.

33.3.2 Source-Receiver Network Geometry

Figure 33.10 shows the location of IMS infrasound array IS44 in relation to potentially active volcanoes in Kamchatka, Russia (Siebert and Simkin 2002-). Although IS44 provided high signal-to-noise ratio infrasound recordings of the June 2009 eruption of Sarychev Peak in the Kuriles (Figs. 33.1, 33.2 and 33.3) and seems to provide numerous observations of infrasound from different volcanoes in Kamchatka spanning multiple years (Fig. 33.10c), discrimination of the volcanic signals and their attribution to a particular volcano is complicated for the Kamchatka region. The complication is the location of multiple potentially active volcanoes lying along similar back azimuth trajectories from IS44 (Fig. 33.10b). Additional regional infrasound array or network deployments in the region would greatly facilitate the detection and discrimination of volcanic sources in Kamchatka.

Global acoustic detection and association capabilities are controlled by the overall network density, as well as the locations and noise levels of critical stations in volcanic regions. We anticipate significant improvements in global detectability of volcanic infrasound in the future as the IMS infrasound network achieves planned 59-station global coverage (Fig. 33.11). Figure 33.11 shows the computed great-circle distances from each potentially active volcano identified in the

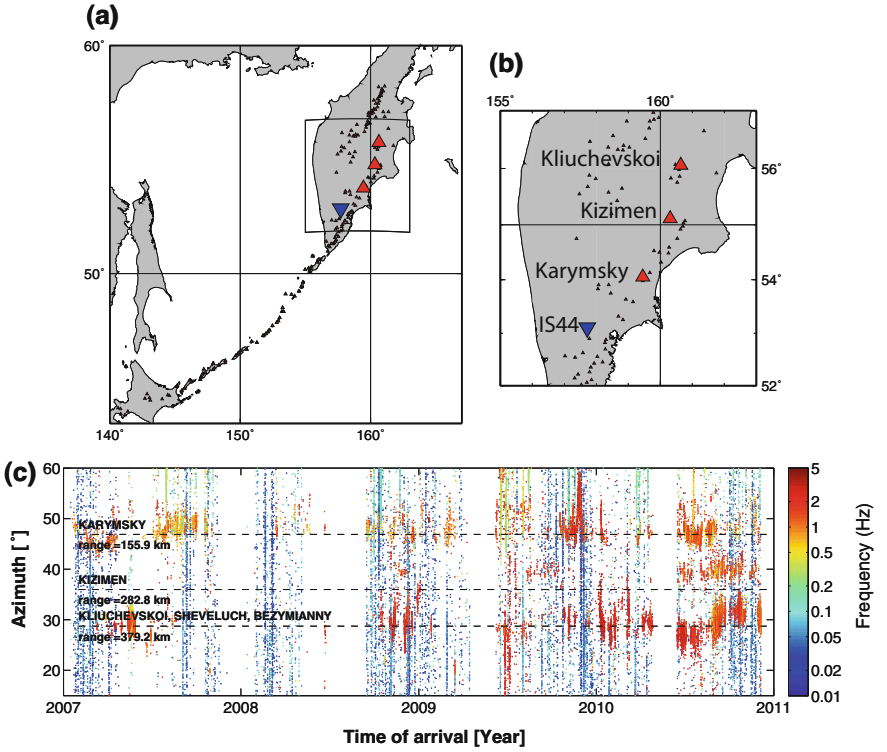

Fig. 33.10 IS44 2007–2010 PMCC results (Matoza et al. 2013) compared to locations of potentially active volcanoes in the Kamchatka and Kuriles regions (red triangles, Siebert and Simkin 2002). **a** and **b** Map of the region with the most active volcanoes labeled. **c** PMCC pixels plotted as a function of time and back azimuth and colored by frequency. Signals with mean frequencies >0.5 Hz (orange and red colors) in (**c**) are possible volcanic signals. Multiple potentially active volcanoes fall along a similar back azimuth trajectory from IS44, complicating the unique attribution of infrasound to a volcanic source given the available network geometry

Smithsonian Global Volcanism Program (GVP) database to the nearest two or three IMS stations, and serves as a first-order proxy for infrasonic network detection capability of global volcanism. Figure 33.11 gives a preliminary view of how volcanic eruption detectability will improve by completing the IMS network and also reveals the volcanic regions (e.g., the Caribbean, Southeast Asia, Aleutians) that would most benefit from additional regional infrasound arrays. Additional infrasound arrays deployed in regions with dense volcanism (e.g., Guilbert et al. 2005; Matoza et al. 2007; Garces et al. 2008; Matoza et al. 2011b; De Angelis et al. 2012; Taisne et al. 2012; Tailpied et al. 2013) will lead to significant improvements by augmenting the network density and decreasing the acoustic source power of explosive eruption detectable with a globally integrated network (Le Pichon et al. 2009; Green and Bowers 2010). In addition to infrasound propagation effects, noise levels experienced by key stations in volcanic regions play an important role in

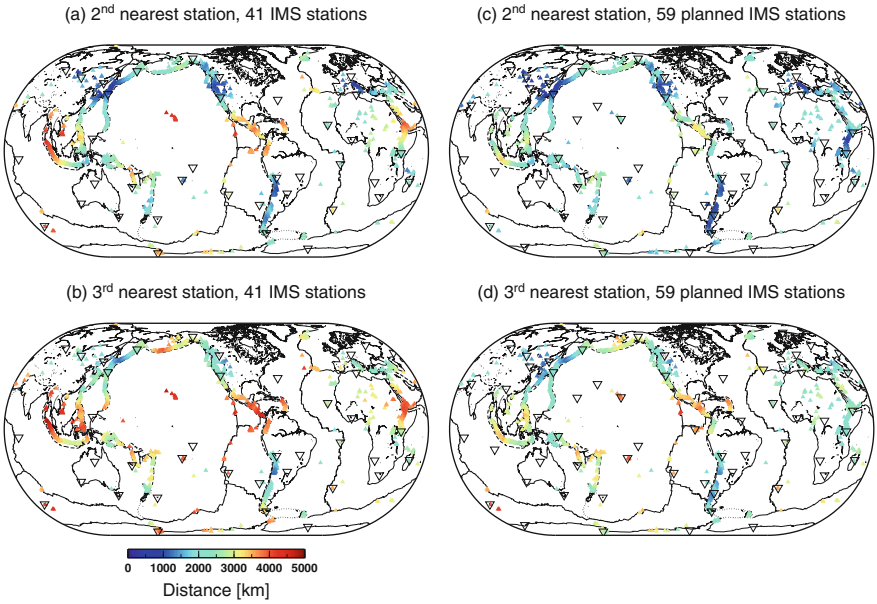

Fig. 33.11 The IMS network and potentially active volcanoes. The distance from each potentially active volcano in the Smithsonian GVP database of Siebert and Simkin (2002-) (inverted triangles with color scale corresponding to distance) are shown with respect to the nearest 2 or 3 IMS stations (open inverted triangles) given (a, b) the 41-station network configuration available from 2005–2010 and (c, d) the planned 59-station IMS network (location of 60th station IS28 is to be determined). The color scale is the same in each case. (Figure reproduced from Matoza et al. 2017)

controlling volcanic signal detection. This is especially the case for island stations, where noise levels are often high and variable; e.g., IS06, Cocos Islands is critical for observing Indonesian volcanoes.

33.4 Diversity of Volcanic Processes and Infrasound

Volcanic processes produce a great diversity of infrasound source mechanisms and signals. The duration of volcanic infrasound waveforms can range from short-duration events lasting ~1 s, to sustained tremor signals lasting months to years. Amplitudes span a wide dynamic range, from small signals approaching the noise level of infrasound sensors [mPa] to larger explosions producing nonlinear shock waves with overpressures exceeding atmospheric pressure ($>10^5$ Pa). Topography and volcanic crater morphology modify the signals and create additional variety (Sect. 33.7). Despite source process diversity and waveform complexity, wavefield modeling and inversion techniques have been used to infer eruption source parameters and processes (e.g., Matoza et al. 2009a; Kim et al. 2015). In this section, we briefly describe the diversity of observed infrasound

signals and highlight imaging and modeling techniques that have been used to characterize and understand volcano infrasound sources. We focus on more recent work in this section; the reader is referred to Johnson and Ripepe (2011) and Fee and Matoza (2013) for more in-depth treatments of these topics.

33.4.1 Low-Viscosity Magmas

Low-viscosity (e.g., basaltic) magmas characteristically exhibit long-lived effusive eruptions punctuated by short explosive bursts, along with occasional gas-rich lava fountaining episodes. Effusive eruptions and roiling lava lakes have been observed to produce near-continuous broadband and/or harmonic infrasound. Kilauea Volcano is a well-studied example with prodigious broadband and harmonic infrasonic tremor and occasional short-duration explosions (e.g., Fee et al. 2010b; Matoza et al. 2010). As another example, lava fountaining from Mount Etna produces high-amplitude, sustained tremor with occasional repeating explosions (e.g., Cannata et al. 2009; Ulivieri et al. 2013).

Of interest for the acoustics of low-viscosity systems is the potential for coupling of the sound field from a magma column into the atmosphere. Buckingham and Garcés (1996), Garcés (2000) and Garcés and McNutt (1997) developed a canonical model, deriving an analytic solution for the airborne Green's function from a resonant magma conduit. To couple the sound field from the magma column to the atmosphere, a near-surface bubbly mixture with high void fraction would lower the impedance contrast between the magma and atmosphere aiding signal transmission (Garcés and McNutt, 1997; Garcés et al. 1998), but may also result in strong attenuation of acoustic waves, hindering transmission (Marchetti et al. 2004). Matoza et al. (2010) proposed that the low-frequency anomalous transparency theory of Godin (2006, 2007) allows infrasound to propagate from a subsurface basaltic magma column into the atmosphere, without requiring a near-surface foam layer.

Cavities and gas-filled conduits above degassing magma bodies also appear to substantially shape the infrasonic signature. The ~200 m cavity above the Halema`uma`u lava lake at Kilauea, Hawaii was modeled as a Helmholtz resonator, producing sustained ~0.5 Hz tremor and explosion pulses (Fig. 33.12) (Fee et al. 2010c), while sustained harmonic tremor from vigorous degassing at the Pu`u O`o cone was attributed to flow-induced oscillations through the shallow cavity structure (Matoza et al. 2010). Similar processes have been invoked at other volcanoes; for example, Villarica, Chile may also generate continuous infrasound through Helmholtz resonance (Goto and Johnson 2011), resonance of a Bessel horn (Richardson et al. 2014), or flow instabilities within the upper conduit (Ripepe et al. 2010b).

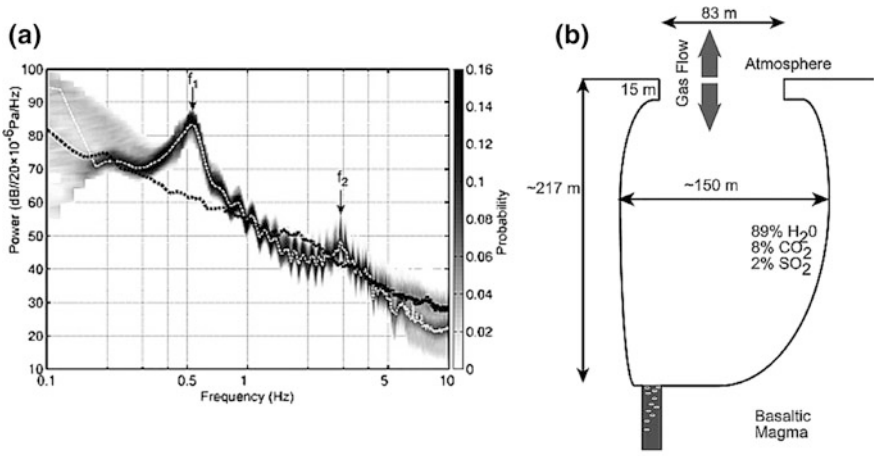

Fig. 33.12 Observed infrasound and its interpretation at Halema`uma`u, Kilauea Volcano (Fee et al. 2010c). **a** Probability density function of the PSD. The dotted white line displays the peak probability, with a dominant peak around 0.55 Hz (f_1) and a secondary peak at ~3 Hz (f_2). The dotted black line represents background noise level. **b** Cartoon of Halema'uma'u cavity, assuming Helmholtz resonance and eigenfunction analysis of a rectangular cavity. The vertical dimension is well constrained from lidar. Comparison of the observed spectra with theoretical modeling suggests that the width of the cavity is variable. (Figures reproduced from Fee et al. 2010c)

33.4.2 Strombolian Eruptions

Strombolian explosions generate short-duration infrasonic signals related to the gas overpressure and gas volume released. Explosions from the archetypical Stromboli Volcano, Aeolian Islands have been studied in particular detail (e.g., Ripepe et al. 2007). The acoustics of Strombolian activity have also been captured at Yasur, Vanuatu (Marchetti et al. 2013), and Mount Erebus (phonolite lava lake "Ray Lake"), Antarctica (Johnson et al. 2008a). Waveforms from Strombolian explosions are characterized by an initial compressional onset followed by a rarefaction, with extended coda reverberation in some cases (e.g., Firstov and Kravchenko 1996; Ripepe et al. 1996; Johnson 2003; Ripepe and Marchetti 2002; Ripepe et al. 2007; Johnson et al. 2008a; Jones et al. 2008). Explosions at Stromboli are understood to result from the coalescence of bubbles in a foam at depth in the conduit, the rise of this gas as a slug flow, and the subsequent bursting of this slug at the magma surface (Harris and Ripepe 2007). Braun and Ripepe (1993) and Ripepe et al. (1996) deployed the first infrasonic microphones at Stromboli, determining that bursting of the large gas bubbles at the surface of the magma column was responsible for simultaneous seismic and acoustic signals. Vergniolle and Brandeis (1994) and Vergniolle et al. (1996) proposed that oscillation of the bubble immediately prior to bursting and kinematic waves on the magma surface after the burst were the significant acoustic sources rather than the bubble burst itself.

Doppler radar observations of Strombolian explosions at Mount Erebus indicate that the bubble does not vibrate prior to bursting (Gerst et al. 2008, 2013). Prior to bursting, a volumetric expansion of the bubble membrane is observed, but the membrane rips before equilibrium pressure is reached (Gerst et al. 2008). Radar, visual, and infrasound data indicate that directivity during bubble rupture can be manifest in the acoustic radiation pattern (Gerst et al. 2008; Johnson et al. 2008a).

33.4.3 Silicic Systems

More viscous magmas are able to build up higher pressures within the conduit and form pressurized solid lava plugs or domes. The destruction of these plugs or domes commonly generates large, ash-rich explosions with sizeable ash plumes and ballistics. The acoustic signals from these eruptions are generally longer in duration, lower frequency, higher amplitude, and more complex than Strombolian explosions (Sect. 33.5.1) (e.g., Ripepe et al. 2010a; Fee et al. 2013b; Yokoo et al. 2013). Exotic infrasound signals are often generated in such systems, perhaps via gas escape through narrowing channels (Fig. 33.13) (Lees et al. 2004).

Hydrothermal and magmatic-hydrothermal interaction processes are also capable of infrasonic signal generation. Infrasonic pulses associated with long-period (LP) seismic events during the 2004–2008 eruption of the stratovolcano Mount St. Helens were attributed by Matoza et al. (2009a) to the repeated rapid pressure loss from a hydrothermal crack by venting into a shallow layer of loosely consolidated, highly permeable material. In this model, heating by magmatic activity causes pressure to rise, periodically reaching the pressure threshold for rupture of a valve sealing the crack. Sudden opening of the valve generates the broadband infrasonic signal and simultaneously triggers the collapse of the crack, initiating resonance of the remaining fluid leading to the seismic LP waveform. Johnson et al. (2008b) used visual, seismic, and geodetic data at Santiaguito Volcano, Guatemala to relate LP events to rapid uplift of a lava dome. The partial collapse of dacitic lava domes (Green and Neuberg 2005; Moran et al. 2008) and explosive blowout of gas-charged blocks impacting the ground (Oshima and Maekawa 2001) generate infrasound, while collapse may depressurize the magmatic system, leading to large explosive eruptions (e.g., Fee et al. 2013b).

Fast-moving, hazardous pyroclastic flows composed of ash and gas have been located and tracked using arrival times and Doppler shift on microphone networks or infrasound arrays (Sect. 33.6.4) (Yamasato 1997; Ripepe et al. 2009; Ripepe et al. 2010a). Lahars, or volcanic mudflows, can also generate infrasound; Johnson and Palma (2015) detected and tracked a large lahar from the 2015 eruption of Villarica Volcano, Chile using a nearby infrasound array. Silicic systems and magmatic-hydrothermal interactions also generate explosive volcanism, which is addressed in Sects. 33.5 and 33.6.

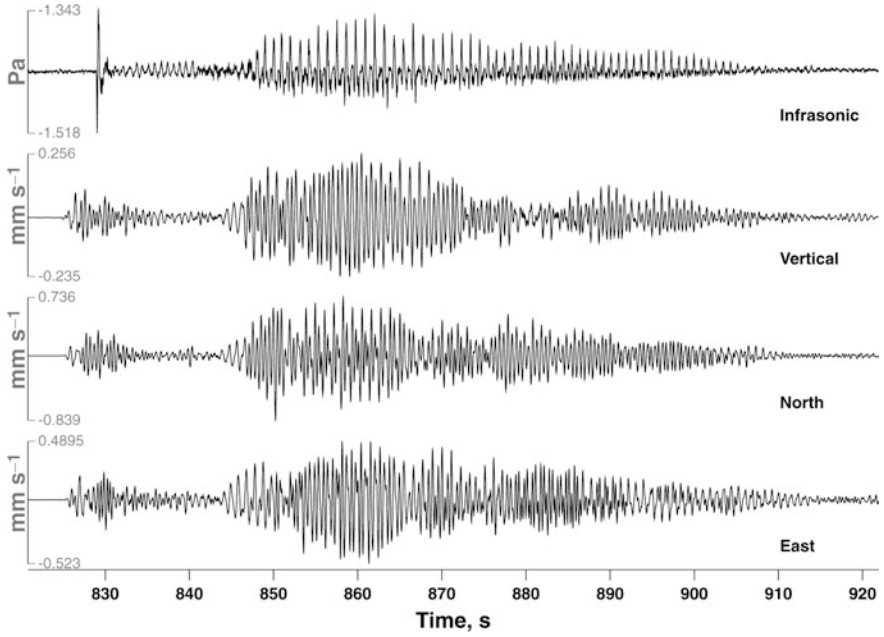

Fig. 33.13 Explosion followed by a sequence of continuous chugging (periodic tremor) at Karymsky Volcano, Kamchatka, Russia (Lees et al. 2004). The top trace is from an infrasonic microphone and the lower three traces are vertical, north, and east seismograms, respectively. (Figure reproduced from Lees et al. 2004)

33.4.4 Imaging Volcano-Infrasonic Sources

Volcano-acoustic studies have an advantage over volcano-seismic studies, in that the source processes are often amenable to direct observation. Visual, infrared (IR), and ultraviolet (UV) imaging synchronized with acoustic instrumentation has enabled a deeper understanding of volcano infrasound sources. High-speed visual (e.g., Yokoo et al. 2009; Genco et al. 2014) and infrared (e.g., Delle Donne and Ripepe 2012) video has been employed to image supersonic shock waves emanating from explosions and reconstruct the resultant acoustic waves. Differencing of images from sustained volcanic jets has revealed repeated shock waves emanating from the edges of the jet (Taddeucci et al. 2014). Imagery provides an independent estimate of the volume flux to constrain acoustic source models. Infrasound-derived gas volumes have been compared to constraints from video (Johnson et al. 2008a; Johnson and Miller 2014), IR (De Angelis et al. 2016), and UV (Dalton et al. 2010; Delle Donne et al. 2016) imagery.

Qualitatively, imagery also helps us to compare eruption styles and eruption parameters derived from infrasonic measurements. Lopez et al. (2013) used visual and infrared imagery, along with infrasound and gas measurements, to identify four

unique eruption styles at Karymsky Volcano, Kamchatka. Combined imagery and acoustic data are also comparable with laboratory and numerical experimental results.

33.4.5 *Experimental Studies of Volcanic Infrasound*

Analog laboratory, theoretical, and computational models have been used to investigate volcano-infrasound signal generation. In particular, the rise and burst of gas slugs and the associated infrasound signals have been investigated. Lane et al. (2013) performed analog experiments and used dimensional analysis to compare the rise and burst of laboratory gas slugs with observed infrasound signals from Strombolian explosions. They found a good qualitative agreement between simulated and observed waveforms, as well as a quantitative correlation between the independently derived gas slug length, mass, and overpressure. Vidal et al. (2010) showed how in laboratory studies, and potentially volcanoes, the complex and unpredictable nature of the slug rupture at the surface may lead to unpredictable source estimates using infrasound.

Explosions within the conduit or shallow subsurface can produce sizeable infrasound signals involving a more complex source process. Analog experiments of explosions underwater and in the shallow subsurface have been performed to investigate acoustic signal generation. Ichihara et al. (2009) analyzed a series of explosions within a lake to better understand the resultant acoustic waves and how they relate to the scaled depth, underwater pressure wave, and motion of the water surface. These observations were then compared to linear acoustic theory, with the observations showing lower amplitudes and higher frequencies than predicted by the theory. Bowman et al. (2014) examined acoustic signals from small subsurface explosions at different burial depths at an outdoor test facility. They observed a sequential three-stage sequence of sound generation due to ground deformation, gas release, and spall slap. These stages are observed from both non-volcanic and volcanic buried explosions (e.g., lava domes and plugs).

Analog modeling of acoustic signals has also been performed to investigate tremor and volcanic explosions in higher viscosity magmas. Lyons et al. (2013) performed flow-driven experiments in which harmonic signals were input into a viscoelastic fluid to simulate volcano-seismic and acoustic tremor. They found that acoustic tremor was produced only when a high fluid stiffness was achieved, allowing a stable pathway for the signals to propagate. This may explain why harmonic infrasonic tremor is only occasionally recorded during periods of harmonic seismic tremor.

33.5 Infrasound from Explosive Volcanism

Explosive eruption processes generate the most energetic infrasound signals associated with volcanoes, and are of most relevance for long-range detection with the IMS. Explosive volcanic eruptions are of immediate interest for their associated societal and economic hazards. Explosive volcanic eruptions are also large, naturally occurring, infrasonic sources, which may be used to validate and improve methods for infrasound propagation modeling, signal detection, discrimination, association, and source location to help improve operational IMS capabilities.

33.5.1 Explosive Volcanism Infrasound Signal Types

Infrasound signals from explosive eruptions capture the rich variety of physical explosion mechanisms (Fig. 33.14). Conceptual understanding of acoustic signals from explosive eruptions has tended to focus on two end-member signal durations: (1) discrete explosion waves with relatively simple waveforms lasting from several to tens of seconds (e.g., Firstov and Kravchenko 1996; Ripepe and Marchetti 2002; Johnson 2003; Marchetti et al. 2009, 2013), and (2) sustained, broadband, infrasonic tremor signals lasting from minutes to hours (e.g., Vergniolle and Caplan-Auerbach 2006; Matoza et al. 2009b; Fee et al. 2010a; Caplan-Auerbach et al. 2010). Commonly, the signals (1) are simply called "explosions" in the volcano acoustics literature and they have been modeled, using linear equivalent source theory (Sect. 33.6.1), as acoustic monopoles, i.e., sources represented as time-varying mass fluxes (e.g., Woulff and McGetchin 1976; Firstov and Kravchenko 1996; Johnson 2003; Delle Donne and Ripepe 2012). However, it is recognized that in many cases these "explosion" waves have nonlinear characteristics (Sect. 33.6.2) (Yokoo and Ishihara 2007; Marchetti et al. 2013; Garces et al. 2013), and nonlinear effects will increase with increasing overpressure release rate and supersonic ejection velocities (Needham 2010). Sustained, broadband infrasonic tremor signals (2) from more sustained eruptions (often described as "Vulcanian," "sub-Plinian," and "Plinian") resemble an infrasonic form of the jet noise produced by smaller scale man-made jets (Matoza et al. 2009b; Fee et al. 2010a, 2013a; Matoza et al. 2013b). Here, for simplicity, we refer to this signal type as *volcanic jet noise* (Sect. 33.6.3).

Observed explosive eruption signals often represent intermediate cases between idealized explosion or blast waves (1) and volcanic jet noise (2), and result from explosive processes that are not adequately described by the type eruption styles (e.g., "Strombolian," "Vulcanian," or "sub-Plinian"). Such complex waveform types appear to be a characteristic feature and behavior of intermediate-composition (andesitic) low-level explosive volcanism. For example, explosions at Sakurajima (Fig. 33.14) are described in papers by Ishihara (1985), Yokoo et al. (2013), and Fee et al. (2014); they are characterized by the rapid explosion of a magma plug and

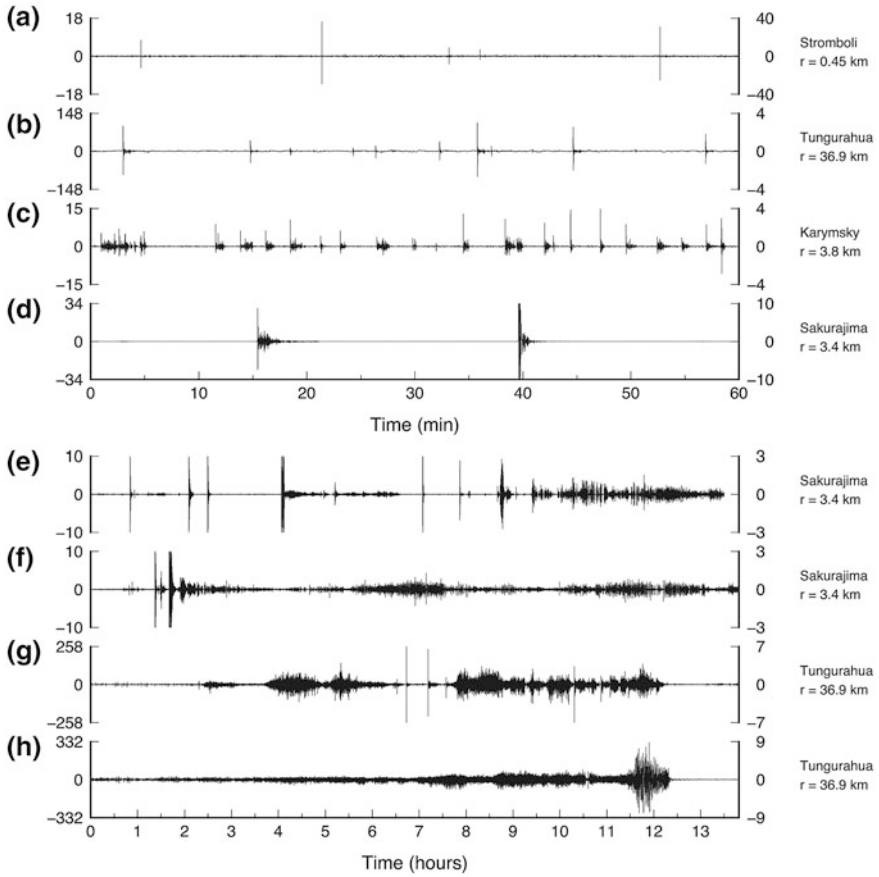

Fig. 33.14 Example infrasonic pressure waveforms associated with different explosive eruptive styles at different volcanoes. The top four traces (a-d) are of 1-hour duration, while the lower four traces (e-h) are of 13.8-hour duration. The right-hand labels indicate the volcano and recording distance (range) r [km]. In each case, the right-hand y-axis is the observed acoustic pressure amplitude at that range, while the left-hand y-axis is the amplitude corrected to a reference distance of 1 km from the source by assuming $1/r$ geometrical spreading for approximate comparison. **a** Typical Strombolian explosions from Stromboli Volcano, Italy (Ripepe and Marchetti 2002). **b** More energetic but still considered "Strombolian" explosions from Tungurahua, Ecuador, with codas containing harmonic tremor (Fee et al. 2010b). **c** Complex explosion waveforms from Karymsky, Kamchatka, with an initial sharp compressional onset followed by short-duration jetting (Lopez et al. 2013) or "blow-off" (Firstov et al. 2013). **d** Complex Vulcanian explosion waveforms at Sakurajima, Japan, similar to those at Karymsky but with longer inter-event times and different amplitudes and coda durations. **e** Complex explosion sequence at Sakurajima, including a mix of discrete explosions, volcanic jet noise, and signals of intermediate type. **f** A different Sakurajima example, more akin to volcanic jet noise but with discrete explosions or shocks interspersed. **g** sub-Plinian eruption from Tungurahua, Ecuador, consisting of multiple sustained sequences of volcanic jet noise interspersed with discrete explosions (Matoza et al. 2009b; Fee et al. 2010b). **h** sub-Plinian to Plinian eruption at Tungurahua: a sustained volcanic jet noise signal with more gradually evolving signal properties. Note: Figs. 33.14d, e, and f have been "clipped" to emphasize lower amplitude explosion codas and jetting; the peak onset compression amplitudes greatly exceed those shown on this plot. (Figure reproduced from Fee and Matoza 2013 and Matoza et al. 2014)

consist of strong acoustic waves, ejection of volcanic bombs, and high ash contents. Similar volcanic explosion complexity has been reported elsewhere, where it has been described variously as (a) "small, ballistic and ash-laden eruptive events," e.g., at Karymsky (e.g., Johnson 2007); (b) "low-intensity explosions" and "weak Vulcanian," e.g., at Santiaguito and Fuego (Guatemala), Villarrica (Chile), and Stromboli (Italy) (e.g., Sahetapy-Engel et al. 2008; Marchetti et al. 2009; Johnson et al. 2008b); or (c) "ash explosion," e.g., at Karymsky (e.g., Lopez et al. 2013; Firstov et al. 2013). Figure 33.14 illustrates selected examples of Sakurajima infrasound data compared to data from other explosive volcanic eruptions (Fee and Matoza 2013; Matoza et al. 2014). Many of the Sakurajima signals resemble "typical" explosion (1) waveforms (Fig. 33.14d–f), but with complex onsets and long-duration codas (tens to hundreds of seconds). Other, more sustained Sakurajima signals are qualitatively closer in character to volcanic jet noise (2, Fig. 33.14e, f), but are not simply a sustained, smoothly time-varying signal; the signals tend to stop and start erratically. In some cases, a sustained jet-noise-like signal is initiated by a more impulsive explosion, while in other cases the sustained signal begins with an emergent onset.

Tephra-rich and gas-rich (tephra poor) explosions have been found to produce quite similar basic waveform metrics (e.g., Fee et al. 2010b; Lopez et al. 2013; Matoza et al. 2014), which would make it challenging to automatically determine ash content based on simple metrics extracted from sparse long-range infrasound data. However, with more local volcano monitoring and dedicated field studies, it may be possible to identify unique waveform properties associated with ash-rich or ash-poor eruptions (e.g., Ripepe and Marchetti 2002; Lopez et al. 2013). Detailed field studies and infrasound waveform modeling, combined with laboratory and numerical studies, may provide eruption velocity source-time functions for this class of low-intensity explosive eruptions, constraining the dynamics of plume ascent and ash dispersal from unsteady eruptions and helping to mitigate societal and economic volcanic hazards.

33.5.2 Infrasound and Satellite-Derived Explosion Chronologies

Explosion chronologies determined from remote infrasound data (e.g., Figure 33.3) provide an independent constraint on eruption chronologies compiled using satellite data (Fee et al. 2010a, b; Matoza et al. 2011a). Comparisons of the two chronologies are relatively straightforward when explosions occur isolated in time. However, comparisons between the two chronologies require a higher level of interpretation when the infrasound detections occur continuously or with short

inter-event times (e.g., between Julian day 163 and 164.5 on Fig. 33.3). Satellite-derived explosion onset times for the June 2009 eruption of Sarychev Peak in Fig. 33.3 were estimated from the time when a dense ash cloud is first visible in satellite data (TERRA, NOAA, MTSAT) above the meteorological cloud layer. However, continuous ash and gas-steam emissions were also observed in satellite data during the eruption, e.g., between Julian day 163 and 164.5. Closely spaced explosions may feed a single sustained eruption column (e.g., Sparks et al. 1997). In addition, pyroclastic flows can generate infrasound (Sect. 33.6.4) (e.g., Yamasato 1997; Ripepe et al. 2009) and not all explosions that generate infrasound produce ash (e.g., Ripepe and Marchetti 2002; Garces et al. 2008; Fee et al. 2010b; Lopez et al. 2013). Therefore, we do not necessarily expect a one-to-one correlation between infrasound signal detections and visual satellite observation of plumes. Furthermore, low-amplitude source activity may not register on remote infrasound stations and weak explosions reaching only low altitudes are more easily obscured in satellite data by cloud cover. Nevertheless, remote infrasound signal detections provide a continuous, high-temporal-resolution chronology of the volcanic source that may be compared with satellite data (Fig. 33.3).

33.5.3 Scaling Between Plume Height and Infrasound

Infrasonic signals have been compared both qualitatively and quantitatively with ash plume height. Johnson et al. (2005) reported a poor correlation between the seismo-acoustic energy release and plume height from small, transient eruptions at Tungurahua Volcano, Ecuador. They concluded that the seismo-acoustic energy partitioning from small eruptions is complex. Fee et al. (2010a) compared acoustic power estimates with ash plume height for a variety of eruption styles at Tungurahua. They found a positive correlation between ash plume height and acoustic power for large, sustained sub-Plinian and Plinian eruptions. Lower frequency infrasound also correlated well with ash plume height from the Plinian eruptions of Kasatochi and Okmok Volcanoes, Alaska (Fee et al. 2010b). Dabrowa et al. (2011) took a comprehensive look at volcanic eruptions recorded on the IMS network, systematically comparing acoustic signal metrics with available ash plume height data. In summary, and similar to other studies of large eruptions, they found that: (1) the distance at which infrasound was recorded increases with ash plume height, (2) the lowest detected infrasonic frequency decreases with increasing plume height, and (3) the total acoustic energy and distance-corrected amplitude increase as a function of plume height.

Numerous authors have built upon the formulation of Lighthill (1978) and Woulff and McGetchin (1976), relating the acoustic source type (monopole, dipole, or quadrupole) and acoustic power to the volcanic jet velocity, and then extrapolating to estimate the plume height (Caplan-Auerbach et al. 2010; Ripepe et al. 2013). However, Matoza et al. (2013b) highlights how the original formulations of

Lighthill (1978) and Woulff and McGetchin (1976) are unlikely to be appropriate for volcanic jet flows, and that estimates of acoustic power at volcanoes are likely incorrect due to undersampling of the directional acoustic wavefield using a standard ground-based monitoring network. A quantitative acoustic source model relating the acoustic wavefield to gas exit velocity and potentially mass flux is needed in order to infer volcanic plume height using infrasound.

33.6 A Closer Look at Explosive Eruption Infrasound

One of the goals of infrasonic volcanic monitoring is to better characterize volcanic eruptions by providing relationships between measured pressure time-series and eruption flow parameters (e.g., Garces et al. 2013 *and references therein*). In order to achieve this, models of acoustic generation (and propagation) are required.

33.6.1 Linear Acoustic Equivalent Sources

The pioneering study by Woulff and McGetchin (1976) introduced the idea of using radiated acoustic power and frequency content to infer gas exit velocity for eruptions involving vigorous release of volcanic gases. This represents a first attempt at a quantitative framework relating volcanic fluid mechanics and acoustic wave generation. Woulff and McGetchin (1976) measured sound-pressure level near volcanic fumaroles. They then used sound-pressure level to estimate the overall sound power level by assuming an acoustic source radiating sound equally in all directions (i.e., no source directionality, spherically symmetric source). Finally, they used results from the classical aeroacoustics literature (Lighthill 1962, 1963; Curle 1955) to relate the total acoustic power to the gas exit velocity for assumed equivalent *monopole*, *dipole*, and *quadrupole* sources. Although Woulff and McGetchin (1976) only considered acoustic signals >20 Hz, recent infrasound studies have built extensively upon their formulation (e.g., Vergniolle et al. 1996, Vergniolle and Caplan-Auerbach 2006; Caplan-Auerbach et al. 2010; Ripepe et al. 2013; Lamb et al. 2015).

The *monopole* is the most elementary linear equivalent source and radiates sound equally in all directions (also called a *simple source* or *point source*). For the monopole, acoustic pressure is related to the rate of change of the rate of mass outflow at the source. The first few seconds of an impulsive volcanic explosion, which involves a rapid acceleration of the atmosphere, are sometimes reasonably well approximated by a monopole (Woulff and McGetchin 1976; Johnson 2003); however, this approximation breaks down as the source amplitude and eruption velocity increase (Sect. 33.6.2). Higher order equivalent sources (dipoles and quadrupoles) can be mathematically constructed from combinations of monopoles (e.g., Morse and Ingard 1968; Lighthill 1962, 1978; Pierce 1989). Woulff and

McGetchin (1976) suggested that such higher order sources might adequately represent fluid-solid interactions (dipole) and aerodynamic sound (quadrupole).

Explosive eruption source mechanisms are likely more complicated than a simple monopole, dipole, or quadrupole assumption. In a reexamination of the approach by Woulff and McGetchin (1976) in the context of the current understanding of jet noise, Matoza et al. (2013b) concluded that the formulation of Woulff and McGetchin (1976) can lead to large errors when inferring eruption parameters from acoustic data and thus requires modification. Quantitative integration of field, numerical, and laboratory studies within a modern aeroacoustics framework will lead to a more accurate relationship between volcanic infrasound and eruption parameters.

33.6.2 Nonlinear Effects

Linear acoustic theory (Sect. 33.6.1) provides a useful starting point for utilizing pressure time-series recordings to estimate eruption parameters. However, it is recognized that supersonic flow at a volcanic vent or a rapid explosive decompression of a pressurized magma-gas mixture can lead to the generation of shock waves, or finite-amplitude acoustic waves, that exhibit nonlinear propagation effects (e.g., Morrissey and Chouet 1997; Johnson 2003; Fee et al. 2013a; Marchetti et al. 2013).

Linear acoustic waves satisfy the small-signal approximation, where pressure fluctuations in the wave are significantly smaller than the product of ambient density and the square of the small-signal sound speed (which for air is comparable to the static pressure, e.g., Blackstock 2000). When this approximation is violated, finite-amplitude effects occur. These effects result in the high-amplitude, higher temperature compressions propagating faster than the small-signal sound speed, progressively leading to a steeper wave onset as the wave develops (see Atchley 2005, for an informative primer).

Explosions generate a high-amplitude positive overpressure phase. In the case of chemical explosions, this is a consequence of the rapid expansion of the gases produced; in a volcanic eruption, it is a combination of rapid mass injection into the atmosphere and the resulting expansion of the gas phase. The nonlinear propagation of this high-amplitude positive pressure perturbation leads to the formation of a waveform often described as a blast wave: a short-duration high-amplitude positive overpressure with a steep onset (the shock front) followed by a quasi-exponential decay and a lower amplitude longer rarefaction phase (e.g., Kinney and Graham 1985). The blast wave elongates during the nonlinear propagation phase (Fig. 33.15) and undergoes faster pressure amplitude decay at short propagation distances when compared to acoustic waves, leading to a relatively rapid transition from nonlinear to approximately linear acoustic propagation.

Volcanic explosions often generate pressure waveforms with the general form of a blast wave (Fig. 33.16). For large Vulcanian explosions, the transition from

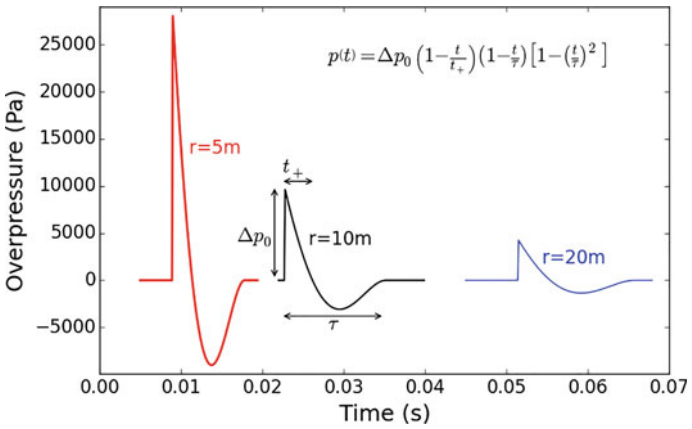

Fig. 33.15 Modeled blast waveforms. The distances correspond to 5 m (red line), 10 m, (black line) and 20 m (blue line) from a 1 kg chemical (TNT) detonation scaled using the Kinney and Graham (1985) reference explosion values for positive overpressure Δp_0 and positive phase duration t_+. The pressure time-series $p(t)$ is calculated using the modified Friedlander equation proposed by Reed (1977), which is given at the top of the figure

nonlinear to approximately linear propagation is expected to occur at several hundred meters from the vent (Medici et al. 2014). Using models that do not account for the initial nonlinear propagation can lead to underestimation of source power (as recognized by, e.g., Caplan-Auerbach et al. 2010; Kim and Rodgers 2016).

Marchetti et al. (2013) noted the similarity between the waveform shape of infrasonic transients recorded at Yasur volcano, Vanuatu, and blast waves recorded from chemical explosions. However, care must be taken to appropriately scale both time and amplitude when comparing with blast waveforms from chemical detonations, as the general waveform shape is characteristic of any nonlinear acoustic propagation from a transient event (Kinney and Graham 1985). In the volcanic case, the positive overpressure phase duration is significantly longer than for blast waves generated by chemical explosives. In Fig. 33.17 a waveform recorded at Sakurajima is compared to an appropriately scaled chemical blast waveform generated using the modified Friedlander function of Reed (1977). This empirically derived blast waveform shape (see Fig. 33.15) was scaled such that the peak overpressure matches the Sakurajima time-series at the recording distance of 3.4 km. It is clear that in the volcanic case the positive pressure pulse is longer for the given peak pressure. Indeed, to match the positive phase duration (~0.7 s for the Sakurajima case, Fig. 33.17), an equivalent surface chemical explosion is required to have a yield of approximately 2,500 tons of TNT. The overpressure expected for a chemical detonation with this pulse length at 3.4 km distance would be on the order

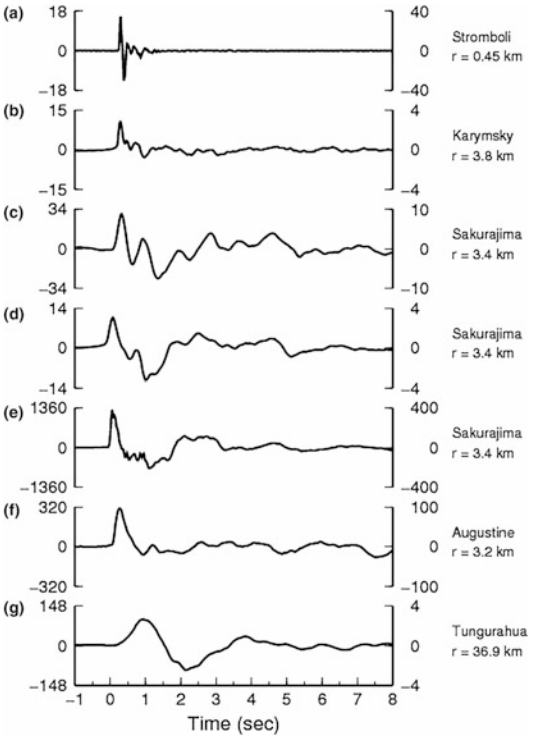

Fig. 33.16 Examples of the onset of transient infrasonic pressure waveforms from different explosive eruption styles at different volcanoes. The right-hand *y*-axis values are the observed pressure amplitude at the station [Pa]. The left-hand *y*-axis values are the amplitudes corrected to a reference distance of 1 km from the source assuming an approximate 1/*r* geometrical spreading for relative comparison. Adapted from Fee and Matoza 2013 and Matoza et al. (2014)

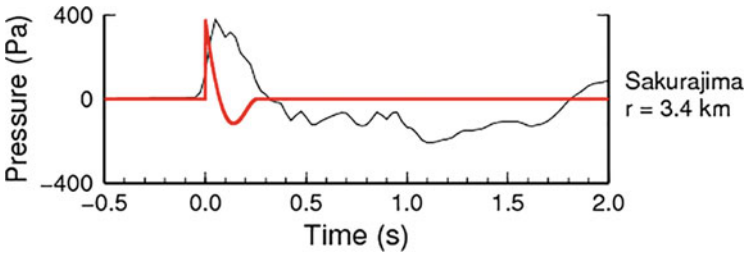

Fig. 33.17 A comparison of a signal recorded at 3.4 km from an explosion at Sakurajima (black line) and the Reed (1977) blast waveform (red line) with peak amplitude matched to the volcanic signal. The positive phase duration of the blast waveform consistent with the peak amplitude was determined using the Kinney and Graham (1985) chemical explosion scaling laws

of 4,300 Pa (i.e., over an order of magnitude higher than observed, Fig. 33.17). As a data example of a chemical explosion of this magnitude, the study by Gainville et al. (2010) describes pressure recordings from a comparable explosion (3,840 tons of TNT equivalent exploded at the surface, equivalent to a 7.6 kt free air explosion). The pulse duration observed by Gainville et al. (2010) was 0.855 s at 7.26 km from the blast, which matches well with the Kinney and Graham (1985) scaling laws. Modeling of volcanic explosions suggests that the longer positive phase duration (e.g., Fig. 33.17) may be a consequence of shock generation within a particle-rich magma–gas mixture in which the small-signal sound speed is slower than that in the atmosphere (Morrissey and Chouet 1997). Near-source topography may also significantly affect the waveform (Sect. 33.7).

Methods to interpret infrasonic recordings using knowledge of near-source nonlinear propagation are starting to be developed (e.g., Medici et al. 2014; Genco et al. 2014). Because infrasonic recordings are most likely to be made in the linear acoustic regime, models are required to relate these measurements to the source that generated the shock waves (as is done in explosion forensics, e.g., Ford et al. 2014; Kim and Rodgers 2016). In order to develop models for volcanic nonlinear acoustic sources, estimation of shock velocities at near-vent locations using visual methods are especially important (e.g., Yokoo and Ishihara 2007; Genco et al. 2014).

Many large eruptions are recorded at global distances from the volcano (e.g., Dabrowa et al. 2011), but interpretation of signal features recorded at these ranges in terms of nonlinear source processes is not trivial. Infrasound propagating within global waveguides reach stratospheric and possibly thermospheric altitudes (50–110 km), where low-density atmosphere is encountered resulting in large-amplitude increases of the acoustic wave. These amplitude increases can be large enough to initiate nonlinear wave propagation (e.g., Lonzaga et al. 2015). Such a mechanism was proposed to explain audible returns at distances of between 100 and 800 km from the 1980 Mount St. Helens eruption (Reed 1987) (see Sect. 33.2.1).

33.6.3 Volcanic Jet Noise

The lowermost section of a sustained sub-Plinian or Plinian volcanic eruption column represents a momentum-driven, turbulent, free-shear jet flow. Recent work has suggested that eruptions involving volcanic jet flows generate a low-frequency (infrasonic) form of the aeroacoustic jet noise produced by smaller scale man-made jets (Matoza et al. 2009b; Fee et al. 2010a, b, 2013a; Taddeucci et al. 2014). Jet noise is the noise generated by a turbulent jet flow itself. Man-made jet noise has

been extensively studied for noise and vibration control purposes (e.g., Tam 1998). Jet noise has been characterized in laboratory and field aeroacoustics studies by considering how acoustic signal properties vary as a function of angle to the jet axis and jet operating parameters such as the jet velocity, diameter, temperature, density, and nozzle geometry. In current jet noise studies, the idea of jet noise as composed of equivalent sources of monopoles, dipoles, and quadrupoles (Sect. 33.6.1) has largely been abandoned (Tam 1998; Tam et al. 2008; Viswanathan 2009). Also of note is that jet noise is highly directional, i.e., jets do not radiate sound equally in all directions.

Although the spectral shapes of observed infrasonic signals are in approximate agreement with those scaled from man-made jets (Matoza et al. 2009b), the observed volcanic signals have additional complexities not present in the pure-air laboratory data. These features may result from multiphase flow containing solid particles and liquid droplets, very high temperatures, and complex crater morphology. Recently, volcanic jet noise has begun to be investigated computationally (Fig. 33.18) (e.g., Taddeucci et al. 2014; Brogi et al. 2015; Cerminara et al. 2016). Taddeucci et al. (2014) combined high-speed imaging with infrasound and seismic observations of jet noise from Strombolian explosions together with numerical simulations. They conclude that both microphone measurements and wave imaging reveal the presence of high-frequency, likely shock-related, jet noise, which they contend to be in agreement with supersonic velocities of pyroclasts measured in some Strombolian explosions (Taddeucci et al. 2012). For more detail about volcanic jet noise, the reader is referred to the paper by Matoza et al. (2013b).

33.6.4 Infrasound from Pyroclastic Flows

Hot, dense, flows of particles and gas, referred to as pyroclastic flows or pyroclastic density currents (PDCs), represent a significant hazard to local populations. These flows have also been found to produce notable infrasound signals (Yamasato 1997; Oshima and Maekawa 2001; Ripepe et al. 2010a, b; Delle Donne et al. 2014). Yamasato (1997) tracked PDCs with seismic and acoustic sensors at Mount Unzen, Japan. At Soufrière Hills Volcano, Montserrat, Ripepe et al. (2010a) characterized, tracked, and estimated velocities of a PDC using a local infrasound array. Delle Donne et al. (2014) built upon this work by integrating thermal and seismic data to further constrain the PDC movement and evolution. Future work relating PDCs and infrasound to understand the acoustic source process has the potential to help mitigate this dangerous volcanic hazard.

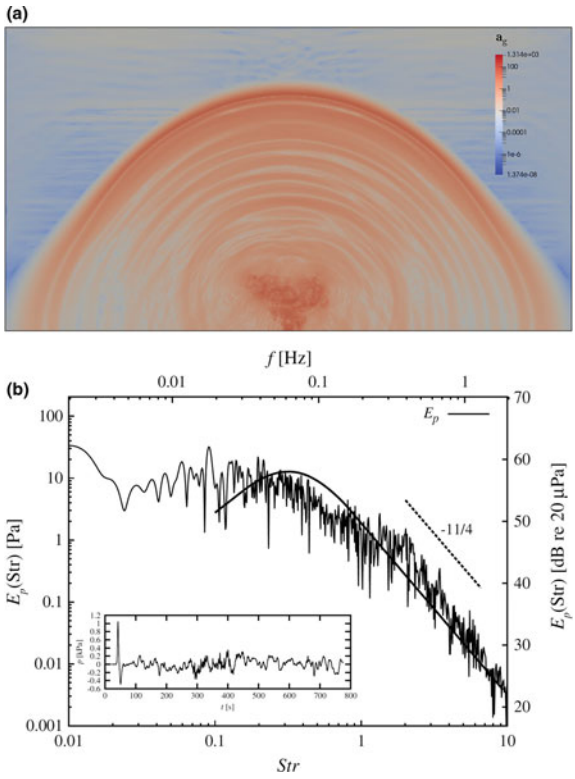

Fig. 33.18 Numerical simulation of infrasound from a volcanic jet (Cerminara et al. 2016). Simulation snapshot showing infrasonic signal generated by turbulent eddies. Infrasound is visualized using the magnitude of the acceleration field with a logarithmic color scale [m/s^2], 120 s after the eruption onset. **b** Infrasonic spectrum of the pressure fluctuations as measured from a probe placed at the ground level 15 km from the vent center. The frequency is expressed in both dimensional (f) and non-dimensional ($Str = fD/U$) forms. The empirically derived large-scale turbulence similarity spectrum is shown by the bold solid line (see Tam 1998). (Figure reproduced from Cerminara et al. 2016)

33.7 Topographic and Near-Source Effects

Before volcanic source parameters can be estimated from infrasound recordings, any acoustic propagation effects between the source and receiver have to be accounted for. Near-source topographic effects may also become convolved with the volcanic source function, complicating the interpretation of long-range

(e.g., IMS) recordings. Characterizing propagation effects in volcanic environments is challenging; modifications to the Green's function (compared to a source within a homogeneous atmospheric halfspace) arise from interactions of the infrasonic wavefield with both along-path topography and meteorologically generated refractive index variations. For example, diffraction and reflection from prominent along-path topographic features, including near-vent structure, results in anisotropic acoustic amplitudes across local infrasound recording networks (e.g., Matoza et al. 2009a; Kim and Lees 2011; Lacanna and Ripepe 2013; Kim and Lees 2014; Kim et al. 2015). In addition, mesoscale meteorological changes can generate significant acoustic ducting variations (e.g., Drob et al. 2010), with infrasonic signal amplitudes varying by over an order of magnitude across periods of a few days (e.g., Fee and Garces 2007; Matoza et al. 2009a; Johnson et al. 2012; Dabrowa et al. 2014; Lacanna et al. 2014).

Prominent topography in volcanic environments (e.g., vents, craters, domes, and ridges) makes it difficult to find non-obstructed propagation paths between a volcanic infrasound source and a local receiver. Acoustic propagation across such topography causes diffraction and reflection resulting in waveform distortion and amplitude variation compared to the wavefield generated by a compact source within a homogeneous halfspace. These effects are described mathematically by a modified Green's function connecting source and receiver, and have been modeled using numerical methods.

Matoza et al. (2009a) simulated the full seismo-acoustic wavefield from a shallow-buried explosive source at Mount St. Helens using a finite-difference method, and showed that the strong crater topography generates an asymmetry in infrasound waveforms radiated in different directions. At Stromboli, time-independent amplitude reductions of up to 11 dB (a factor of 3.5) compared to hemispherical acoustic spreading are observed, over path lengths of several hundred meters (Lacanna and Ripepe 2013). Finite-difference acoustic modeling using rigid topography (no seismic wavefield) indicates that the source of the amplitude reductions is primarily along-path topographic diffraction and reflections.

Kim and Lees (2014) investigated topographically generated waveform distortion at Sakurajima Volcano, Japan, with source-to-receiver path lengths between 2 and 7 kilometers. They observed amplitude reductions at most stations (of up to 8 dB compared to hemispherical spreading), but also observed a repeatable amplitude increase (~2 dB) at one station. Finite-difference time-domain (FDTD) modeling, accounting for 3D effects, successfully simulated both the amplitude reductions and increases (Fig. 33.19). These studies indicate that the superposition of along-path acoustic diffraction and reflection effects, especially those generated close to the active vent, need to be understood in order to interpret absolute infrasonic amplitudes.

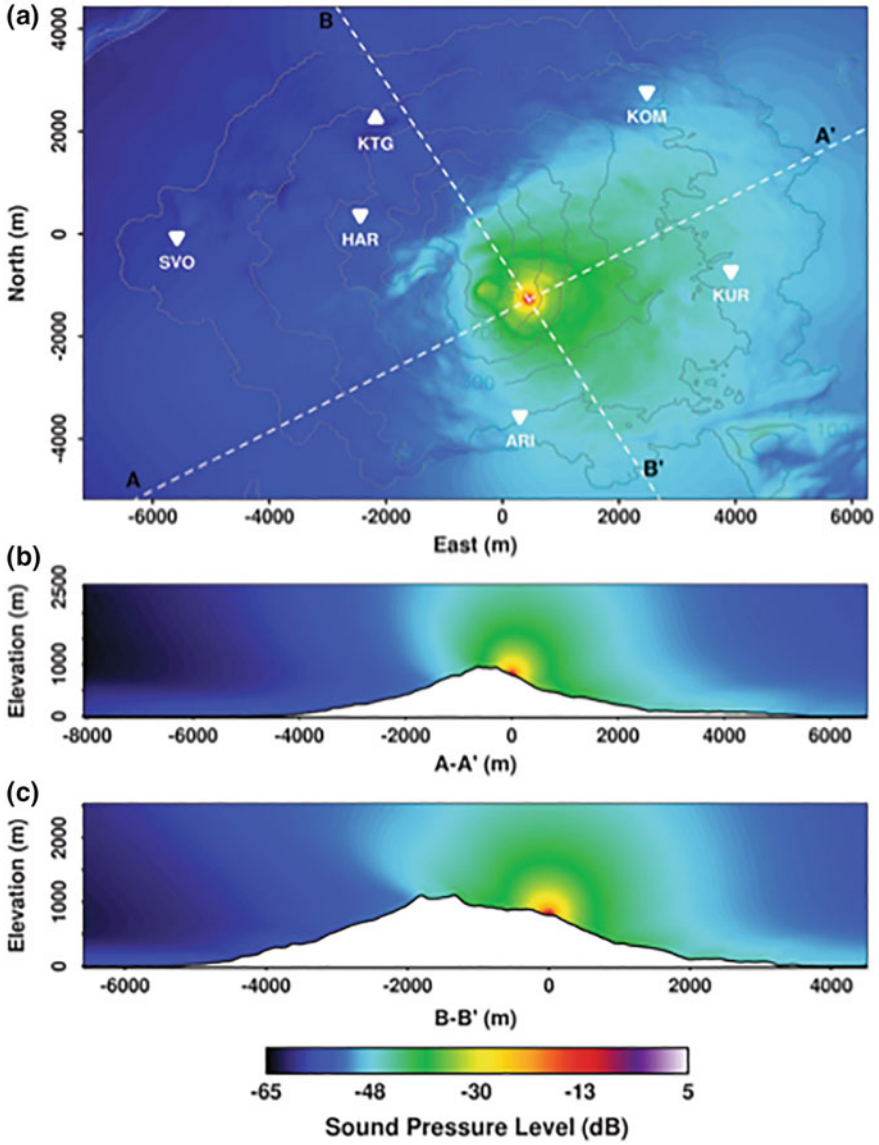

Fig. 33.19 An example of asymmetric sound pressures levels (SPL) due to the influence of along-path topography at Sakurajima Volcano (Kim and Lees 2014). The SPL is relative to the pressure 10 m from the source and is computed using a 3D FDTD simulation. (Figure reproduced from Kim and Lees 2014)

Topographically generated waveform distortion can also have a large effect on the estimation of explosive source parameters that are of potential use to the volcano monitoring community, such as volume flux. Kim et al. (2015) compare volume flux inversions using both (1) the standard approximation of the acoustic pressure being only a function of source strength and source-to-receiver distance, and (2) a full 3D numerical calculation of the Green's function using FDTD and a high resolution digital elevation model. Their results indicate that if 3D structure is neglected along a relatively unobstructed source-to-receiver path at Sakurajima, the total volume flux for a typical explosive event is underestimated by ~50%.

Although topography dominates short path (<5 km) amplitude reductions at volcanoes with relatively simple sources (e.g., Stromboli, Lacanna and Ripepe 2013), at volcanic dome complexes the acoustic wavefield may be a superposition of spatially separated sources. This is a potential additional source of anisotropic acoustic radiation (e.g., Jones and Johnson 2011). This adds extra complexity when interpreting infrasonic waveforms at some silicic volcanoes.

In addition to generating amplitude variations, topographic obstacles can generate waveform time delays. Kim and Lees (2014) show that for stations with prominent along-path topographic blockages at Sakurajima, time delays of greater than 0.5 s are observed over distances of ~4.5 km compared to those expected for a single-velocity, no-topography model. These delays can be predicted using 3D FDTD simulations with accurate volcanic topography models. This allowed Kim and Lees (2014) to locate a series of ten typical explosions at Sakurajima within a tight cluster (<100 m radius) at the base of the active crater, consistent with thermal infrared source vent locations. In a similar manner, Rowell et al. (2014) illustrate the difficulties in resolving the altitude of high-frequency jetting sources when time delays generated by topography are not accounted for.

Over propagation paths of several kilometers, atmospheric rather than topographic controls begin to dominate the variations in observed infrasonic signal characteristics. When considering infrasound propagation, the most significant of these effects are (1) refraction from vertical gradients in temperature and wind (e.g., Reynolds 1878), and (2) scattering from turbulence (e.g., Ostashev 1997). Sound absorption at low frequencies (<10 Hz) is negligible along short path lengths (<20 km) and little energy is lost to the ground such that surface impedance effects can be neglected (e.g., Piercy et al. 1977; Sutherland and Bass 2004). To first order, infrasonic propagation is controlled by temperature and wind gradients, while turbulence may result in additional fluctuations in signal amplitude and phase.

Infrasonic propagation from volcanic vents to local stations at distances less than 20 km is confined to the atmospheric boundary layer, where temperature and wind variations can result in variable acoustic ducting and can lead to significant waveform distortion. For example, Matoza et al. (2009a) observed rapid evolution of infrasonic waveforms recorded 13.4 km from the source at Mount St. Helens (as quantified by the cross-correlation coefficient). This evolution was attributed to changes in microscale and mesoscale meteorology (i.e., propagation conditions)

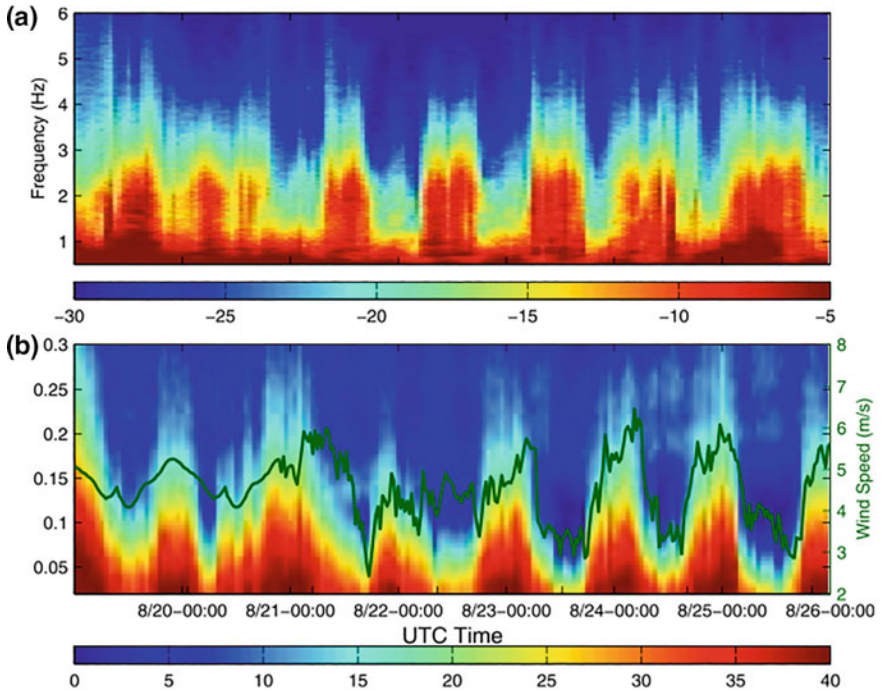

Fig. 33.20 Beamed spectrograms between **a** 0.5 and 6 Hz and **b** 0.02 and 0.3 Hz for infrasound signals at an array ~12.5 km from an active vent at Kilauea, Hawaii (Fee and Garces 2007). Spectral amplitudes are given in dB re 1 Pa. Panel **b** indicates the wind speed recorded at a nearby tower as a green line, showing that low-frequency acoustic power is indicative of increased wind speeds. The volcanic signal is observed between 1 and 3 Hz in (**a**) and indicates that favorable propagation conditions occur during low-wind, stable nocturnal conditions. (Figure reproduced from Fee and Garces 2007)

rather than source location or source-time function (as is often the case when analyzing seismic signals).

Variable acoustic ducting results in large variations in signal amplitudes between source/receiver pairs. Unfavorable propagation conditions, where acoustic energy undergoes strong upward refraction into the upper atmosphere, can lead to non-detection of signals at stations located several to tens of kilometers from the vent. Fee and Garces (2007) observed an order-of-magnitude diurnal variation in infrasonic tremor signal power at 12.5 km from the active vent at Kilauea, most likely generated by the formation and dissipation of an acoustic waveguide within the stable nocturnal atmospheric boundary layer (Fig. 33.20). Over a longer time period of 2 weeks, Dabrowa et al. (2014) observed over an order-of-magnitude variation in signal amplitude decay across a 25 km propagation path at Mount Erebus, which was well-correlated with mesoscale variations in lower atmospheric wind and temperature gradients recorded by local radiosondes. During periods of increased negative sound speed gradients with altitude, increased upward refraction

of infrasonic energy leads to lower recorded amplitude levels at 25 km from the vent. Such studies show that time- and location-specific meteorological data is required in order to be able to successfully interpret changes in infrasonic amplitudes at these ranges. One method of estimating near-volcano meteorological conditions is to use collected infrasound data. If the microbarograph network density is sufficient, and there is an almost continuous volcanic infrasound signal, estimates of the near-surface sound speed gradients and wind vector may be estimated from inter-station phase delays (Marcillo and Johnson 2010) and acoustic power fluctuations (Johnson et al. 2012).

33.8 Regional-Global Infrasound Propagation

Due to efficient low-frequency acoustic energy propagation within the atmosphere, eruptions at over 40 volcanoes have been recorded across the IMS global infrasound network over the past 15 years (see Fig. 33.7 and e.g., Le Pichon et al. 2005; Dabrowa et al. 2011). The more intense eruptions have been recorded on multiple arrays out to distances of several thousands of kilometers (e.g., Fee et al. 2010a; Matoza et al. 2011a; Fee et al. 2013a).

Regional and global infrasound recordings have helped constrain chronologies for eruptive sequences in situations where there are no local ground-based recording instruments (e.g., Matoza et al. 2011a), where only part of the eruptive sequence is subaerial (e.g., Green et al. 2013), and where local instruments have been destroyed by the onset of an intense eruption (e.g., Caudron et al. 2015). The continuous nature of infrasound recordings is also important; for the 2009 Sarychev Peak, Kuriles, eruption Matoza et al. (2011a) used a 5-day long infrasound time-series to corroborate, and improve upon, a satellite imagery based chronology that had a lower temporal resolution.

Propagation of infrasound out to thousands of kilometers from the source occurs because the acoustic waves are channeled within ducts between the ground and the upper atmosphere (e.g., Georges and Beasley 1977). Unlike local infrasonic recordings where the sound has propagated exclusively through the lower troposphere, regional and global infrasound will have propagated up into the stratosphere, mesosphere, or lower thermosphere before being refracted back to Earth's surface. This refraction is the result of refractive index increases generated by a combination of increased temperature and/or along-path wind speed. Drob et al. (2010a) provide an overview of the major propagation ducts: the stratospheric duct where acoustic energy reaches a maximum altitude of between 35 and 55 km, and the thermospheric duct where infrasound returns to the ground surface from altitudes of between 90 and 120 km. The majority of long-range infrasound propagates within the stratospheric duct, because thermospheric paths suffer from significantly

higher acoustic attenuation (Sutherland and Bass 2004). Propagation within the stratospheric duct is highly anisotropic; the winds associated with the stratospheric polar vortex assist in channeling energy propagating in a downwind direction, while refracting acoustic energy up into the thermosphere along upwind paths (e.g., Le Pichon et al. 2012). As infrasonic energy passes through layers with rapidly varying windspeeds in the stratosphere, the waves undergo multi-pathing and scattering (Kulichkov 2004), such that the recorded wavefield at long-range is comprised of a superposition of multi-pathed wavefronts (Green 2015).

Given the complexities of long-range infrasound propagation within the atmosphere, and the impact this has upon the radiated wavefield, identifying eruption characteristics from acoustic recordings at long distance is challenging. Despite this, progress has been made in identifying volcanic source characteristics using long-range infrasound recordings. Regional infrasound studies have shown that as eruptive intensity increases, with the consequence of higher altitude plume generation, the dominant infrasonic signal frequency decreases (often to below 0.1 Hz) resulting in wider signal bandwidths and greater radiated acoustic power (e.g., Garces et al. 2008; Fee et al. 2010b). Similar relationships are observed at global distances; for infrasound recordings made across the IMS from over 65 volcanic eruptions, events with higher altitude plumes generated lower detectable signal frequencies (Dabrowa et al. 2011). Acoustic source characteristics are sometimes identifiable at long range, especially if the propagation path is relatively simple. For example, Fee et al. (2013b) observe infrasound at 260 km from the intense 2011 eruption of Nabro Volcano, Eritrea, consistent with energy propagation up to the lower thermosphere, where it is refracted back to the station. The signal exhibits positively skewed infrasonic waveforms, which the authors interpret as similar to "crackle," a phenomenon that is indicative of supersonic jet noise.

Uncertainties in the source to receiver propagation path result in uncertainties in both source location and origin time. For both the Sarychev Peak and Eyjafjallajökull eruptions, source location estimates using back azimuth intersection of long-range infrasound recordings have mean centroids that can be several tens of kilometers away from the volcanic source (Matoza et al. 2011a, b). For some phases of the 2008 Kasatochi, Alaska, eruption Fee et al. (2010a) identify discrepancies of ~15 min between origin times derived using either infrasonic or seismic data; they interpret these differences as being due to possible mis-identification of the atmospheric duct through which the infrasound propagated.

As many volcanoes are sources of strong and persistent infrasound, volcano infrasound has been extensively used for remote sensing of the upper atmosphere. The long duration (weeks, months, years) of volcanic infrasound activity has allowed (1) the identification of periodic fluctuations in infrasonic signal characteristics, (2) infrasound signals to be used to validate meteorological and climatological specifications, and (3) estimation of updates to upper atmosphere meteorological specifications (i.e., wind vectors) by minimizing the difference between observed and predicted signal characteristics.

Semi-diurnal fluctuations in regional volcanic infrasound amplitudes (Le Pichon et al. 2005), trace velocities (Matoza et al. 2011a) and travel-times (Assink et al. 2012) have been shown to correlate well with expected tidal fluctuations in the turning height of thermospheric infrasonic propagation paths. Likewise, diurnal fluctuations in signal amplitude and trace velocity over a 10-day period at approximately 2000 km from Eyjafjallajökull were generated by solar tidal fluctuations in windspeeds that modulated the strength of the stratospheric acoustic duct (Green et al. 2012). By using volcanoes with known, fixed locations these studies have allowed higher fidelity comparisons with numerical propagation predictions compared to earlier studies that used microbarom and rocket-generated infrasound to identify tidal signatures (e.g., Donn and Rind 1971; Donn et al. 1975).

Infrasound recordings of continuously erupting explosive volcanoes provide an opportunity to compare observed signal characteristics with those predicted using numerical models and state-of-the-art atmospheric specifications. Studies of one year of explosions from Yasur Volcano, Vanuatu led Le Pichon et al. (2005) to conclude that current meteorological specifications are inadequate for accurately predicting observed thermospheric arrival azimuthal deviations of up to 10°. Specifically, these authors showed that mesospheric zonal winds are underestimated in the models by between 20 and 50 m/s. In contrast, Antier et al. (2007) studied stratospheric arrivals from Yasur over a 3-year period and showed that the meteorological profiles at altitudes below 55 km are accurate enough to account for the observed values and variations in travel-time, trace velocity and back azimuth during the Austral summer months. Le Pichon et al. (2010) extended this study and showed that state-of-the-art meteorological specifications are excellent at predicting back azimuth variations over timescales of between a few days and a few months. For more than 90% of the time, the error between observed and predicted back azimuths is less than 0.5° for this particular summertime stratospheric propagation path. At other times of year, the meteorological specifications are less capable of predicting observed infrasound characteristics; using data from Etna, Assink et al. (2014) showed that trace-velocity observations at times of atmospheric transition (e.g., the equinoxes) can only be modeled by increasing the effective sound speed at the stratopause by up to 10% of the original atmospheric specification value.

Inversion techniques that use infrasound observations to improve high-altitude meteorological profiles have been proposed (Drob et al. 2010b; Lalande et al. 2012), and well-characterized ground-truth signals, such as those collected from volcanoes, allow such inversions to be undertaken in practice. Assink et al. (2013) showed that although variations in observed thermospheric arrival travel-times from eruptions of Tungurahua, Ecuador, correlate with the phase of the thermospheric semi-diurnal tides, the travel-time observations do not match those predicted by numerical modeling. The predicted travel-time discrepancies result in predicted

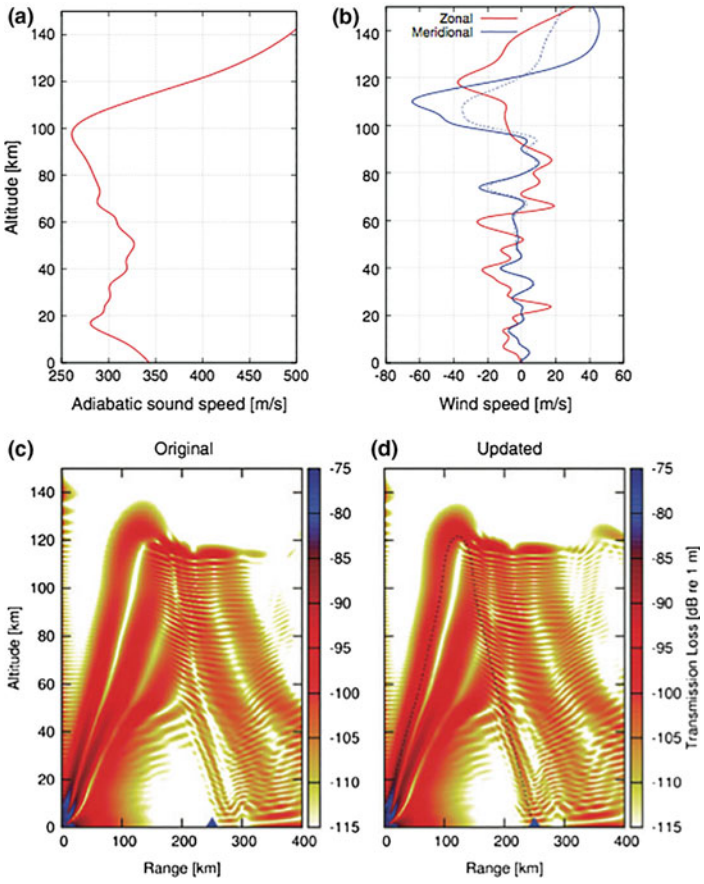

Fig. 33.21 An example, from Assink et al. (2013), of undertaking a wind-speed parameter update (solid lines, panel b) from an original meteorological specification (dashed lines, panel b) in order to explain the occurrence and arrival times of thermospheric arrivals at the LITE array 250 km from Tungurahua, Ecuador (blue triangle, panels c and d). The original specifications predict that the station is at the edge of the thermospheric shadow zone, while the updated specification indicates that a thermospheric arrival turning at an altitude of approximately 120 km is received at the station. (Figure adapted and updated from Assink et al. 2013)

celerities almost 10% lower than observed. Therefore Assink et al. (2013) employed an inversion procedure to identify the best-fitting low-order (four-parameter) wind model in the upper mesosphere and lower thermosphere using the recorded regional thermospheric phases from individual explosions (Fig. 33.21). The results indicate that such an approach provides a physically realistic updated atmospheric profile.

This updated profile was used to correctly predict the nonlinear distortion of the waveform along the path, providing confidence that the inversion method improved the prediction of the true thermospheric propagation path.

These studies highlight that volcano infrasound has the potential to contribute to upper atmospheric remote sensing efforts. Encouragingly, Assink et al. (2014) showed that the amplitudes of the required updates to the windspeeds are consistent with those predicted from other measurements (e.g., lidar).

33.9 Acoustic Early Warning Systems for Explosive Volcanic Eruptions

Infrasound can provide detailed constraints on the timing, duration, and relative vigor of local and remote explosive volcanism (Sects. 33.5, 33.6) and has been used in prototype eruption early warning systems (e.g., Kamo et al. 1994; Garces et al. 2008; Ripepe et al. 2009; Fee et al. 2010a; Matoza et al. 2011a; De Angelis et al. 2012; Fee and Matoza 2013; Marchetti et al. 2019; Ripepe and Marchetti 2019). A global infrasonic *Volcanic Information System* (or VIS) is currently being developed in support of the Volcanic Ash Advisory Centers (VAACs) designated by the International Civil Aviation Organization (ICAO) (Mialle et al. 2015). The VAACs are specialized operational centers responsible for producing and disseminating information on volcanic ash clouds that may endanger aviation, as defined by the International Airways Volcano Watch (IAVW) (Tupper et al. 2007). As such, the VAACs explore opportunities for enhancing their operational capabilities.

The first proposal for an acoustic early warning system for explosive eruptions of which we are aware was that of Kamo et al. (1994), who noted that the Kariya array, 710 km from Sakurajima (see Sect. 33.2.1), was capable of detecting infrasound from volcanoes thousands of kilometers distant (e.g., the 1991 eruption of Pinatubo, Philippines). Kamo et al. (1994) concluded that "this capability forms the basis of a proposal for a worldwide network of air-wave sensors to monitor volcanic explosions," proposing the PEGASAS-VE early warning system consisting of a set of infrasonic microphone arrays with 500–1,000 km spacing. Kamo et al. (1994) proposed that PEGASAS-VE "would be a very effective means of enhancing aviation safety and would be similar to the tsunami warning system, which is in worldwide operation." PEGASAS-VE was not constructed, but the IMS infrasound network was initiated after the CTBT was opened for signature in 1996. The proposed 500-km spacing of PEGASAS-VE was chosen to provide timely warnings within 30 min. For reference, the average station spacing for the complete IMS infrasound network will be about 2,000 km (Christie and Campus 2010).

The Acoustic Surveillance for Hazardous Eruptions (ASHE) project was initiated after the third international workshop on volcanic ash and aviation safety in Toulouse (2003), in which ICAO requested that State Signatories of the CTBT

investigate the use of the IMS for eruption warnings. During this project, two infrasound arrays were deployed near Mount St. Helens (Matoza et al. 2007), and two in Ecuador (Garces et al. 2008; Fee et al. 2010b). The initial goal of the ASHE project was to determine the feasibility of detecting significant atmospheric ash emissions acoustically and rapidly notifying civil defense authorities (ideally, within 5 min).

The ASHE proof-of-concept project demonstrated that acoustic array monitoring of large volcanic eruptions at regional distances is not only viable, but also sufficiently mature to transition into operational volcano monitoring. The ASHE experiment in Ecuador developed an operational monitoring tool for the highly active Tungurahua Volcano using an infrasound array ~37 km away. Fee et al. (2010b) describe how multiple eruptions and a variety of eruption styles were used as case studies to construct the system. Sustained, low-frequency infrasound was found to correspond with hazardous ash plumes (Sect. 33.5.3), while short-duration explosions were found to be primarily gas-rich and/or produce low-level ash plumes. A sub-Plinian eruption on February 6, 2008 was subsequently detected by the ASHE system ~6 min after the eruption onset and a notification to civil aviation authorities was distributed. Changes in the eruption intensity and the eruption cessation were also detected and additional notifications were disseminated. This project demonstrated that acoustic early warning of hazardous eruptions is indeed feasible, even at regional distances (tens of km).

The combination of numerous active volcanoes and its stark remoteness makes Alaska (AK) a prime target for volcano infrasound monitoring. After extensive research showing that significant infrasound is produced from eruptions in Alaska (e.g., Wilson and Forbes 1969; Vergniolle and Caplan-Auerbach 2006; Fee et al. 2010b, 2013b), as well as demonstrating its utility in eruption monitoring, the Alaska Volcano Observatory (AVO) began using infrasound operationally in the early 2010s. De Angelis et al. (2012) describe how both a remote infrasound array and ground-coupled airwaves (GCA) recorded on seismometers from a nearby seismic network were used to detect explosions from the remote Cleveland Volcano, AK. These methods, even with the infrasound array at nearly 1,000 km range, were able to detect numerous eruptions from Cleveland Volcano that were previously going undetected using satellite remote sensing. GCA methods have also been helpful in detecting and characterizing activity at the difficult-to-monitor, but often-active Pavlof Volcano, AK (Waythomas et al. 2014, Fee et al. 2016). Currently, numerous infrasound array and GCA algorithms are running to detect explosive activity from volcanoes in Alaska and produce email and SMS alerts, and the technology is being implemented further with more stations and detection algorithms.

While the utility of infrasound technology for monitoring large explosive eruptions has been demonstrated for specific case studies or regions (e.g., the current operational system in Alaska), the transition to a global approach remains a challenge. Building upon research programs and moving toward achieving an operational VIS, the Comprehensive Nuclear-Test-Ban Treaty Organization

(CTBTO) is coordinating a two-way approach in order to set up the framework agreement for creating the VIS and its technical implementation.

The international framework agreement is being discussed between the CTBTO, ICAO, and the World Meteorological Organization (WMO). ICAO collaborates closely with the WMO on aviation safety issues associated with hazardous weather. Both organizations coordinate activities and generate VAAC advisories on the detection of volcanic ash clouds and their transport and dispersion in the atmosphere because of their potential impact on aviation (e.g., Casadevall et al. 1994). In parallel, the International Data Center (IDC) of the CTBTO informed the Air Navigation Bureau of ICAO that it was working on a "significant eruption" notification system within the ARISE (Atmospheric dynamics Research InfraStructure in Europe) project together with VAAC Toulouse. This project is mandated by IAVW to work on the link between infrasound technology and VAAC activities. The cooperation between the international organizations is further strengthened by a 2011 agreement between the CTBTO and WMO that permits the sharing of data for development activities that are of substantial interest to both parties.

The VIS technical implementation has now been initiated utilizing synergy between the CTBTO, ARISE, and VAAC Toulouse. The IMS infrasound network allows for global remote monitoring of volcanic activity, which permits notifying the international civil aviation community regarding significant volcanic eruptions in near-real time using IDC automatic processing results. The CTBTO provides an operational, robust, and sustainable environment with high-quality infrasound data and derived products, being reinforced by ARISE-advanced products that provide valuable parametric inputs on the atmosphere dynamics that drives the infrasound wave propagation. The combined results are to serve as quality indicators increasing the VAACs confidence when receiving VIS messages.

The first version of the VIS is a two-step process, similar to the IDC automatic processing. First, at the station level, the VIS searches the matching IDC infrasound detections within a database of known volcanoes using simple criteria on detection time of arrival, back azimuth and central frequency for ranges up to 4,000 km and combines it with atmospheric ducting propagation metrics based on the effective sound speed ratio (Le Pichon et al. 2012). Subsequently, the VIS is consolidated at the network level by associating detections from various stations and aggregating detection parameters into eruptive sequences, rather than overloading the VAAC with redundant messages from an ongoing eruption.

This proposed approach is undergoing testing with the VAAC Toulouse using the CTBTO vDEC (virtual Data Exploitation Centre: https://www.ctbto.org/specials/vdec/) platform to demonstrate the usefulness of infrasonic data to the IAVW. While the disseminated information initially focuses on straightforward criteria, it is envisioned to be an iterative process that will later be enriched with advanced research parameters from ARISE and from the international volcano-acoustic scientific community. For example, the multi-year eruptive sequences at Mount Etna, Sicily have been tracked using IMS data from IS48 in Tunisia based on a propagation probability criterion which combines an empirical attenuation relation (Le Pichon et al. 2012) and atmospheric uncertainty estimation

(Tailpied et al. 2013). This example from Mount Etna shows how additional data and parameters are expected to help further enhance and validate the VIS performance.

The initial system serves as a demonstration of the utility of the VIS prior to its possible extension to other VAACs. Looking ahead, support from the volcano-infrasound community is critical in order to lower the volcanic detection threshold and reduce the latency of the VIS. The addition of regional and local infrasound data from volcanic areas and the refinement of the system criteria with state-of-the-art results from the scientific community will help with VIS sustainability.

In line with the goal of the global VIS, Matoza et al. (2017) developed a new alternative algorithm for searching systematically through multi-year data from the IMS infrasound network to identify explosive volcanic eruption signals originating anywhere on Earth. Detecting, quantifying, and cataloging the global occurrence of explosive volcanism helps toward several goals in Earth sciences and has direct applications in volcanic hazard mitigation for both regional (e.g., Alaska) and global (e.g., VIS) systems. The new algorithm by Matoza et al. (2017) combines infrasound signal association across multiple stations with source location using a brute-force, grid-search, cross-bearings approach. The algorithm corrects for a background prior rate of coherent unwanted infrasound signals (clutter) in a global grid, without needing to screen array processing detection lists from individual stations prior to association. This algorithm was developed using case studies of explosive eruptions: 2008 Kasatochi, AK; 2009 Sarychev Peak, Kuriles; and 2010 Eyjafjallajökull, Iceland. They applied the method to global IMS data from 2005–2010 to construct a preliminary acoustic catalog that emphasizes sustained explosive volcanic activity. This work represents a step toward the goal of integrating IMS infrasound data products into global volcanic eruption early warning, parameter estimation, and notification systems.

33.10 Conclusions

Infrasound monitoring is becoming an established geophysical technique for capturing local and remote explosive volcanism, and for understanding the dynamics of shallow degassing and eruption columns. Infrasound signals are recorded from a broad spectrum of volcanic processes ranging from effusive to explosive eruptions. Explosive eruptions produce powerful broadband (~0.01–20 Hz) infrasound signals that can be ducted efficiently over long ranges (thousands of kilometers) in atmospheric waveguides. Although not designed for the purpose, the construction of the IMS is providing an unprecedented opportunity to study and monitor Earth's explosively erupting volcanoes using a global network of ground-based acoustic sensors. The utility of the IMS network for detecting, locating, and providing detailed chronologies of remote explosive volcanism is well established. The

initiation of the global Volcanic Information System (VIS) provides a formal context for research on the improved use of infrasound data for estimating parameters of remote explosive volcanism using the global IMS network. Major research goals in-line with this objective include: (1) continued development of quantitative source models linking acoustic signal generation to eruption parameters, (2) improved propagation modeling of infrasound from sustained broadband sources in a time-varying atmosphere at multiple scales, and (3) the development of robust detection algorithms for identifying and locating volcanic eruption signals in the presence of wind noise and multiple interfering coherent ambient sources. We anticipate significant improvements in the global detectability of volcanic infrasound using the IMS network in the future as the IMS infrasound network achieves planned 59-station global coverage. Additional infrasound arrays or network deployments in volcanically active regions will lead to substantial improvements by augmenting the network density and decreasing the acoustic source power of explosive eruptions detectable with a globally integrated network.

Acknowledgements This work was partially supported by NSF grants EAR-1546139 and EAR-1614855.

References

Annen C, Wagner JJ (2003) The impact of volcanic eruptions during the 1990s. Nat. Hazards Rev 4(4):169–175. https://doi.org/10.1061/(asce)1527-6988(2003)4:4(169

Antier K, Le Pichon A, Vergniolle S, Zielinski C, Lardy M (2007) Multiyear validation of the NRL-G2S wind fields using infrasound from Yasur. J Geophys Res 112:D23110. https://doi.org/10.1029/2007JD008462

Assink JD, Waxler R, Drob D (2012) On the sensitivity of infrasonic traveltimes in the equatorial region to theatmospheric tides. J Geophys Res Atmospheres 117.D01110. https://doi.org/10.1029/2011JD016107

Assink JD, Waxler R, Frazier WG, Lonzaga J (2013) The estimation of upper atmospheric wind model updates from infrasound data. J Geophys Res 118:1–18. https://doi.org/10.1002/jgrd.50833

Assink JD, Le Pichon A, Blanc E, Kallel M, Khemiri L (2014) Evaluation of wind and temperature profiles from ECMWF analysis on two hemispheres using volcanic infrasound. J Geophys Res 119. https://doi.org/10.1002/2014jd021632

Atchley AA (2005) Not your ordinary sound experience: a nonlinear-acoustics primer. Acoust Today 1(1):19–24

Banister JR (1984) Pressure wave generated by the Mount St. Helens eruption. J Geophys Res Atmospheres 89(D3):4895–4904

Båth M (1982) Atmospheric waves from Mount St. Helens. EOS Trans AGU 63(11):193–193

Blackstock DT (2000) Fundamentals of physical acoustics. Wiley-Interscience

Bolt BA, Tanimoto T (1981) Atmospheric oscillations after the May 18, 1980 eruption of Mount St. Helens EOS Trans AGU. 62(23):529–530

Bowman DC, Taddeucci J, Kim K, Anderson JF, Lees JM, Graettinger AH, Sonder I, Valentine GA (2014) The acoustic signatures of ground acceleration, gas expansion, and spall fallback in experimental volcanic explosions. Geophys Res Lett 41(6):1916–1922. https://doi.org/10.1002/2014GL05932

Braun T, Ripepe M (1993) Interaction of seismic and air waves as recorded at Stromboli volcano. Geophys Res Lett 20:65–68

Brogi F, Malaspinas O, Bonadonna C, Chopard B, Ripepe M (2015) Towards a numerical description of volcano aeroacoustic source processes using Lattice Boltzmann strategies. EOS Trans AGU Fall Meet Suppl Abstract S53D-04

Buckingham MJ, Garcés MA (1996) Canonical model of volcano acoustics. J Geophys Res Solid Earth 101(B4):8129–8151

Cansi Y (1995) An automatic seismic event processing for detection and location: the PMCC method. Geophys Res Lett 22(9):1021–1024

Cannata A, Montalto P, Privitera E, Russo G, Gresta S (2009) Tracking eruptive phenomena by infrasound: May 13, 2008 eruption at Mt. Etna. Geophys Res Lett 36:L05304. https://doi.org/10.1029/2008gl036738

Caplan-Auerbach J, Bellesiles A, Fernandes JK (2010) Estimates of eruption velocity and plume height from infrasonic recordings of the 2006 eruption of Augustine Volcano, Alaska. J Volcanol Geoth Res 189(1):12–18

Casadevall TJ (ed) (1994) Volcanic ash and aviation safety: proceedings of the first international symposium on volcanic ash and aviation safety. US Geolo Sur Bull 2047

Caudron C, Taisne B, Garces M, Le Pichon A, Mialle P (2015) On the use of remote infrasound and seismic stations to constrain the eruptive sequence and intensity for the 2014 Kelud eruption. Geophys Res Lett 42. https://doi.org/10.1002/2015gl064885

Cerminara M, Ongaro TE, Neri A (2016) Large Eddy Simulation of gas–particle kinematic decoupling and turbulent entrainment in volcanic plumes. J Volcanol Geotherm Res 326:143–171. https://doi.org/10.1016/j.jvolgeores.2016.06.018

Chester DK, Degg M, Duncan AM, Guest JE (2000) The increasing exposure of cities to the effects of volcanic eruptions: a global survey. Environ Hazards 2(3):89–103. https://doi.org/10.1016/S1464-2867(01)00004-3

Christie D, Campus P (2010) The IMS infrasound network: design and establishment of infrasound stations. In: Pichon AL, Blanc E, Hauchecorne A (eds) Infrasound monitoring for atmospheric studies. chap. 2. Springer, Netherlands, pp 29–75

Cochran E, Shearer P (2006) Infrasound events detected with the Southern California seismic network. Geophys Res Lett 33(19)

Chouet BA, Matoza RS (2013) A multi-decadal view of seismic methods for detecting precursors of magma movement and eruption. J Volcanol Geotherm Res 252:108–175. https://doi.org/10.1016/j.jvolgeores.2012.11.013

Curle N (1955) The influence of solid boundaries upon aerodynamic sound. Proc R Soc London Ser A 231(1187):505–514

Dabrowa AL, Green DN, Rust AC, Phillips JC (2011) A global study of volcanic infrasound characteristics and the potential for long-range monitoring. Earth Planet Sci Lett 310:369–379. https://doi.org/10.1016/j.epsl.2011.08.027

Dabrowa AL, Green DN, Johnson JB, Phillips JC, Rust AC (2014) Comparing near-regional and local measurements of infrasound from Mount Erebus, Antarctica: implications for monitoring. J Volcanol Geotherm Res 288:46–61. https://doi.org/10.1016/j.volgeores.2014.10.001

Dalton MP, Waite GP, Watson IM, Nadeau PA (2010) Multiparameter quantification of gas release during weak Strombolian eruptions at Pacaya Volcano, Guatemala. Geophys Res Lett 37:L09303. https://doi.org/10.1029/2010gl042617

De Angelis S, Fee D, Haney M, Schneider D (2012) Detecting hidden volcanic explosions from Mt. Cleveland Volcano, Alaska with infrasound and ground-coupled airwaves. Geophys Res Lett 39:L21312. https://doi.org/10.1029/2012GL053635

De Angelis S, Lamb O, Lamur A, Hornby A, Aulock F, Chigna G, Lavallée Y, Rietbrock A (2016) Characterization of moderate ash-and-gas explosions at Santiaguito volcano, Guatemala, from infrasound waveform inversion and thermal infrared measurements. Geophys Res Lett 43 (12):6220–6227

Delclos C, Blanc E, Broche P, Glangeaud F, Lacoume JL (1990) Processing and interpretation of microbarograph signals generated by the explosion of Mount St. Helens. J Geophys Res Atmos 95(D5):5485–5494

Delle Donne D, Ripepe M, De Angelis S, Cole PD, Lacanna G, Poggi P, Stewart R (2014) Chapter 9 Thermal, acoustic and seismic signals from pyroclastic density currents and Vulcanian explosions at Soufrière Hills Volcano, Montserrat. Geolo Soc Lon Mem 39(1):169–178

Delle Donne D, Ripepe M (2012) High-frame rate thermal imagery of Strombolian explosions: implications for explosive and infrasonic source dynamics. J Geophys Res Solid Earth (1978–2012):117(B9)

Delle Donne D, Ripepe M, Lacanna G, Tamburello G, Bitetto M, Aiuppa A (2016) Gas mass derived by infrasound and UV cameras: implications for mass flow rate. J Volcanol Geoth Res 325:169–178

Dibble RR, Kienle J, Kyle PR, Shibuya K (1984) Geophysical studies of Erebus Volcano, Antarctica, from 1974 December to 1982 January. NZ J Geol Geophys 27(4):425–455

Donn WL, Rind D (1971) Natural Infrasound as an Atmospheric Probe. Geophys J R Astr Soc 26:111–133

Donn WL, Balachandran NK, Rind D (1975) Tidal wind control of long-range rocket infrasound. J Geophys Res 80(12):1662–1664

Donn WL, Balachandran NK (1981) Mount St. Helens eruption of 18 May 1980: air waves and explosive yield. Science 213(4507):539–541

Drob DP, Garces M, Hedlin M, Brachet N (2010a) The temporal morphology of infrasound propagation. Pure Appl Geophys 167:437–453. https://doi.org/10.1007/s00024-010-0080-6

Drob DP, Meier RR, Picone JM, Garces MM (2010b) Inversion of infrasound signals for passive atmospheric remote sensing. In: infrasound Monitoring for Atmospheric Studies, pp 701–731. https://doi.org/10.1007/978-1-4020-9508-5_24

Dzurisin D (2006) Volcano deformation: new geodetic monitoring techniques. Springer-Verlag, Berlin Heidelberg

Evers LG, Haak HW (2001) Listening to sounds from an exploding meteor and oceanic waves. Geophys Res Lett 28(1):41–44

Fairfield C (1980) OMSI sound project: the acoustic effects of the Mount St. Helens eruption on May 18 1980. Oregon Geol 42(12):200–202

Fee D, Garces M (2007) Infrasonic tremor in the diffraction zone. Geophys Res Lett 34:L16826. https://doi.org/10.1029/2007GL030616

Fee D, Steffke A, Garces, M (2010a) Characterization of the 2008 Kasatochi and Okmok eruptions using remote infrasound arrays. J Geophys Res Atmos 115(D2). https://doi.org/10.1029/2009jd013621

Fee D, Garces M, Steffke A (2010a) Infrasound from Tungurahua Volcano 2006–2008: Strombolian to Plinian eruptive activity. J Volcanol Geotherm Res 193:67–81. https://doi.org/10.1016/j.jvolgeores.2010.03.006

Fee D, Garces M, Patrick M, Chouet B, Dawson P, Swanson D (2010b) Infrasonic harmonic tremor and degassing bursts from Halema'uma'u Crater, Kilauea Volcano, Hawaii. J Geophys Res 115:B11316. https://doi.org/10.1029/2010JB007642

Fee D, Matoza RS (2013) An overview of volcano infrasound: from hawaiian to plinian, local to global. J Volcanol Geotherm Res 249:123–139. https://doi.org/10.1016/j.jvolgeores.2012.09.002

Fee D, Matoza RS, Gee KL, Neilsen TB, Ogden DE (2013a) Infrasonic crackle and supersonic jet noise from the eruption of Nabro Volcano, Eritrea. Geophys Res Lett 40:1–5. https://doi.org/10.1002/grl.5082

Fee D, McNutt SR, Lopez TM, Arnoult KM, Szuberla CAL, Olson JV (2013b) Combining local and remote infrasound recordings from the 2009 Redoubt Volcano eruption. J Volcanol Geotherm Res 259:100–114

Fee D, Yokoo A, Johnson JB (2014) Introduction to an open community infrasound dataset from the actively erupting Sakurajima Volcano, Japan. Seismol Res Lett 85(6):1151–1162

Fee D, Haney M, Matoza R, Szuberla C, Lyons J, Waythomas C (2016), Seismic envelope-based detection and location of ground-coupled airwaves from volcanoes in Alaska. Bull Seismol Soc Am 106:3. https://doi.org/10.1785/0120150244

Firstov PP, Kravchenko NM (1996) Estimation of the amount of explosive gas released in volcanic eruptions using air waves. Volcanol Seismol 17:547–560

Firstov PP, Fee D, Makhmudov ER (2013) The explosive activity of Karymskii Volcano, Kamchatka: Acoustic andseismic observations. J Volcanol Seismol 7(4):252–264

Ford SR, Rodgers AJ, Xu H, Templeton DC, Harben P, Foxall W, Reinke RE (2014) Partitioning of seismoacoustic energy and estimation of yield and height-of-burst/depth-of-burial for near-surface explosions. Bull Seismol Soc Am 104(2):608–623

Gabrielson T (2010) Krakatoa and the Royal Society: the Krakatoa explosion of 1883. Acoust Today 6(2):14–19

Gainville O, Blanc-Benon P, Blanc E, Roche R, Millet C, Le Piver F, Despres B, Piserchia, PF (2010) Misty picture: a unique experiment for the interpretation of the infrasound propagation from large explosive sources. In: infrasound monitoring for atmospheric studies, Springer Netherland, pp 575–598

Garces MA, McNutt SR (1997) Theory of the airborne sound field generated in a resonant magma conduit. J Volcanol Geotherm Res 78:155–178

Garces MA, Hagerty MT, Schwartz SY (1998) Magma acoustics and time-varying melt properties at Arenal Volcano, Costa Rica. Geophys Res Lett 25:2293–2296

Garces M, Iguchi M, Ishihara K, Morrissey M, Sudo Y, Tsutsui T (1999) Infrasonic precursors to a Vulcanian eruption at Sakurajima Volcano, Japan. Geophys Res Lett 26:2537–2540

Garces MA (2000) Theory of acoustic propagation in a multi-phase stratified liquid flowing within an elastic-walled conduit of varying cross-sectional area. J Volcanol. Geotherm. Res 101(1):1–17

Garcés M, Harris A, Hetzer C, Johnson J, Rowland S, Marchetti E, Okubo P (2003) Infrasonic tremor observed at Kīlauea Volcano, Hawai'i. Geophys Res Lett 30(20)

Garces M et al (2008) Capturing the acoustic fingerprint of stratospheric ash injection. EOS Trans AGU 89(40):377

Garces MA, Fee D, Matoza R (2013) Volcano acoustics, chapter 16. In: Fagents SA, Gregg TKP, Lopes RMC (eds) Modeling volcanic processes: the physics and mathematics of volcanism. Cambridge University Press

Genco R, Ripepe M, Marchetti E, Bonadonna C, Biass S (2014) Acoustic wavefield and Mach wave radiation of flashing arcs in strombolian explosion measured by image luminance. Geophys Res Lett 41(20):7135–7142

Georges TM, Beasley WH (1977) Refraction of infrasound by upper-atmospheric winds. J Acoust Soc Am 61(1):28–34

Gerst A, Hort M, Kyle PR, Vöge M (2008) 4D velocity of Strombolian eruptions and man-made explosions derived from multiple Doppler radar instruments. J Volcanol Geoth Res 177 (3):648–660

Gerst A, Hort M, Aster RC, Johnson JB, Kyle PR (2013) The first second of volcanic eruptions from the Erebus volcano lava lake, Antarctica—energies, pressures, seismology, and infrasound. J Geophys Res Solid Earth 118(7):3318–3340

Glasstone S (ed) (1977) The effects of nuclear weapons, *US Department of Defense*

Godin OA (2006) Anomalous transparency of water-air interface for low-frequency sound. Phys Rev Lett 97:164301. https://doi.org/10.1103/PhysRevLett.97.164301

Godin OA (2007) Transmission of low-frequency sound through the water-to-air interface. Acoust Phys 53(3):305–312. https://doi.org/10.1134/S1063771007030074

Goerke VH, Young JM, Cook RK (1965) Infrasonic observations of the May 16, 1963, volcanic explosion on the Island of Bali. J Geophys Res 70(24):6017–6022

Gorshkov GS (1960) Determination of the explosion energy in some volcanoes according to barograms. Bull Volcanol 23:141–144

Gossard EE and Hooke WH (1975) Waves in the atmosphere: atmospheric infrasound and gravity waves: their generation and propagation. Elsevier, Amsterdam

Goto A, and Johnson JB (2011) Monotonic infrasound and Helmholtz resonance at Volcan Villarrica (Chile). Geophys Res Lett 38. https://doi.org/10.1029/2011gl046858
Green DN, Neuberg J (2005) Seismic and infrasonic signals associated with an unusual collapse event at the Soufrière Hills volcano, Montserrat. Geophys Res Lett 32(7)
Green DN, Bowers D (2010) Estimating the detection capability of the International Monitoring System infrasound network. J Geophys Res 115:D18116. https://doi.org/10.1029/2010JD014017
Green DN, Matoza RS, Vergoz J, Le Pichon A (2012) Infrasonic propagation from the 2010 Eyjafjallajökull eruption: investigating the influence of stratospheric solar tides. J Geophys Res 117:D21202. https://doi.org/10.1029/2012JD017988
Green DN, Evers LG, Fee D, Matoza RS, Snellen M, Smets P, Simons D (2013) Hydroacoustic, infrasonic and seismic monitoring of the submarine eruptive activity and sub-aerial plume generation at South Sarigan, May 2010. J Volcanol Geotherm. Res 257:31–43. https://doi.org/10.1016/j.jvolgeores.2013.03.006
Green DN (2015) The spatial coherence structure of infrasonic waves: analysis of data from International Monitoring System arrays. Geophys J Int 201(1):377–389. https://doi.org/10.1093/gji/ggu495
Guilbert J, Harjadi P, Purbawinata M, Jammes S, Le Pichon A, Feignier B (2005) Monitoring of Indonesian volcanoes with infrasound: preliminary results. In: Infrasound technology workshop, Tahiti
Hagerty MT, Schwartz SY, Garces MA, Protti M (2000) Analysis of seismic and acoustic observations at Arenal Volcano, Costa Rica, 1995-1997. J Volcanol Geotherm Res 101:27–65
Harkrider DG (1964) Theoretical and observed acoustic-gravity waves from explosive sources in the atmosphere. J Geophys Res 69(24):5295–5321
Harkrider D, Press F (1967) The Krakatoa air-sea waves: an example of pulse propagation in coupled systems. Geophys J Int 13(1–3):149–159
Harris A, Ripepe M (2007) Synergy of multiple geophysical approaches to unravel explosive eruption conduit and source dynamics–A case study from Stromboli. Chemie der Erde-Geochemistry 67(1):1–35
Ichihara M, Ripepe M, Goto A, Oshima H, Aoyama H, Iguchi M, Tanaka K, Taniguchi H (2009) Airwaves generated by an underwater explosion: implications for volcanic infrasound. J Geophys Res-Solid Earth 114:B03210. https://doi.org/10.1029/2008jb005792
Ichihara M, Takeo M, Yokoo A, Oikawa J, Ohminato T (2012) Monitoring volcanic activity using correlation patterns between infrasound and ground motion. Geophys Res Lett 39:L04304. https://doi.org/10.1029/2011GL050542
Iguchi M (2013) Magma movement from the deep to shallow Sakurajima Volcano as revealed by geophysical observations. Bull Volcanol Soc Japan 58(1):1–18
Iguchi M, Ishihara K (1990) Comparison of earthquakes and airshocks accompanied with explosive eruptions at Sakurajima and Suwanosejima volcanoes (in Japanese). Annu Disas Prev Res Inst Kyoto Univ 33B–1:1–11
Ishihara K (1985) Dynamical analysis of volcanic explosion. J Geodyn 3:327–349. https://doi.org/10.1016/0264-3707(85)90041-9
Johnson JB (2003) Generation and propagation of infrasonic airwaves from volcanic explosions. J Volcanol Geoth Res 121(1):1–14
Johnson JB (2007) On the relation between infrasound, seismicity, and small pyroclastic explosions at KarymskyVolcano. J Geophys Res Solid Earth 112:B08203. https://doi.org/10.1029/2006JB004654
Johnson JB, Ruiz MC, Lees JM, Ramon P (2005) Poor scaling between elastic energy release and eruption intensity at Tungurahua Volcano, Ecuador. Geophys Res Lett 32(15)
Johnson JB, Malone SD (2007) Ground-coupled acoustic airwaves from Mount St. Helens provide constraints on the May 18, 1980 eruption. Earth Planet Sci Lett 258 (1–2):16–31
Johnson J, Aster R, Jones KR, Kyle P, McIntosh B (2008a) Acoustic source characterization of impulsive Strombolian eruptions from the Mount Erebus lava lake. J Volcanol Geoth Res 177 (3):673–686. https://doi.org/10.1016/j.jvolgeores.2008.06.028

Johnson JB, Lees JM, Gerst A, Sahagian D, Varley N (2008b) Long-period earthquakes and co-eruptive dome inflation seen with particle image velocimetry. Nature 456(7220):377–381
Johnson JB, Ripepe M (2011) Volcano infrasound: a review. J Volcanol Geotherm Res 206(3):61–69
Johnson JB, Anderson J, Marcillo O, Arrowsmith S (2012) Probing local wind and temperature structure using infrasound from Volcan Villarrica (Chile). J Geophys Res 117:D17107. https://doi.org/10.1029/2012JD017694
Johnson JB, Miller AJ (2014) Application of the monopole source to quantify explosive flux during vulcanian explosions at Sakurajima Volcano (Japan). Seismol Res Lett 85(6):1163–1176
Johnson JB, Palma JL (2015) Lahar infrasound associated with Volcán Villarrica's 3 March 2015 eruption. Geophys Res Lett 42(15):6324–6331
Jones KR, Johnson JB, Aster R, Kyle PR, McIntosh WC (2008) Infrasonic tracking of large bubble bursts and ash venting at Erebus volcano, Antarctica. J Volcanol Geoth Res 177(3):661–672
Jones KR, Johnson JB (2011) Mapping complex vent eruptive activity at Santiaguito, Guatemala using network infrasound semblance. J Volcanol Geotherm Res 199:15–24. https://doi.org/10.1016/j.volgeores.2010.08.006
Kamo K, Ishihara K, Tahira M (1994) Infrasonic and seismic detection of explosive eruptions at Sakurajima volcano, Japan, and the PEGASAS-VE early-warning system. In: Proceedings of the first international symposium on volcanic ash and aviation safety, U.S. Geological Survey Bulletin 2047, pp 357–365
Kanamori H, Mori J, Harkrider DG (1994) Excitation of atmospheric oscillations by volcanic eruptions. J Geophys Res 99(B11):21947–21961
Kim K, Lees JM (2011) Finite-difference time-domain modeling of transient infrasonic wavefields excited by volcanic explosions. Geophys Res Lett 38:L06804. https://doi.org/10.1029/2010GL046615
Kim K, Lees JM (2014) Local volcano infrasound and source localization investigated by 3D simulation. Seismol Res Lett 85(6):1177–1186. https://doi.org/10.1785/0220140029
Kim K, Fee D, Yokoo A, Lees JM (2015) Acoustic source inversion to estimate volume flux from volcanic explosions. Geophys Res Lett 42:5243–5249. https://doi.org/10.1002/2015GL064466
Kim K, Rodgers A (2016) Waveform inversion of acoustic waves for explosion yield estimation. Geophys Res Lett 43(13):6883–6890
Kinney GF, Graham KJ (1985) Explosive shocks in air. Springer Science & Business Media
Kulichkov SN (2004) Long-range propagation and scattering of low-frequency sound pulses in the middle atmosphere. Meteorol Atmos Phys 85:47–60. https://doi.org/10.1007/s00703-003-0033-z
Lacanna G, Ripepe M (2013) Influence of near-source volcano topography on the acoustic wavefield and implication for source modeling. J Volcanol Geotherm Res 250:9–18. https://doi.org/10.1016/j.volgeores.2012.10.005
Lacanna G, Ichihara M, Iwakuni M, Takeo M, Iguchi M, Ripepe M (2014) Influence of atmospheric structure and topography on infrasonic wave propagation. J Geophys Res 119:2988–3005. https://doi.org/10.1002/2013JB010827
Lalande J-M, Sebe O, Landes M, Blanc-Benon P, Matoza RS, Le Pichon A, Blanc E (2012) Infrasound data inversion for atmospheric sounding. Geophys J Int 190:687–701
Lamb H (1911) On atmospheric oscillations. Proc R Soc Lond Ser A 84(574):551–572
Lamb OD, De Angelis S, Lavallée Y (2015) Using infrasound to constrain ash plume rise. J Appl Volcanol 4(1):1
Landès M, Ceranna L, Le Pichon A, Matoza RS (2012) Localization of microbarom sources using the IMS infrasound network. J Geophys Res 117:D06102. https://doi.org/10.1029/2011JD016684
Lane SJ, James MR, Corder SB (2013) Volcano infrasonic signals and magma degassing: first-order experimental insights and application to Stromboli. Earth Planet Sci Lett 377–378:169–179. https://doi.org/10.1016/j.epsl.2013.06.048
LeConte J (1884) Atmospheric waves from Krakatoa. Science 3(71):701–702

Lees JM, Gordeev EI, Ripepe M (2004) Explosions and periodic tremor at Karymsky volcano, Kamchatka, Russia. Geophys J Int 158(3):1151–1167

Lees JM, Johnson JB, Ruiz M, Troncoso L, Welsh M (2008) Reventador Volcano 2005: eruptive activity inferred from seismo-acoustic observation. J Volcanol Geoth Res 176(1):179–190

Le Pichon A, Blanc E, Drob D, Lambotte S, Dessa JX, Lardy M, Bani P, Vergniolle S (2005) Infrasound monitoring of volcanoes to probe high-altitude winds. J Geophys Res 110:D13106. https://doi.org/10.1029/2004JD005587

Le Pichon A, Vergoz J, Blanc E, Guilbert J, Ceranna L, Evers L, Brachet N (2009) Assessing the performance of the International Monitoring System infrasound network: geographical coverage and temporal variabilities. J Geophys Res 114:D08112. https://doi.org/10.1029/2008JD010907

Le Pichon A, Vergoz J, Cansi Y, Ceranna L, Drob D (2010) Contribution of infrasound monitoring for atmospheric remote sensing. In: infrasound monitoring for atmospheric studies, p 629–646. https://doi.org/10.1007/978-1-4020-9508-5_20

Le Pichon A, Ceranna L, Vergoz J (2012) Incorporating numerical modeling into estimates of the detection capability of the IMS infrasound network. J Geophys Res 117:D05121. https://doi.org/10.1029/2011JD016670

Lighthill MJ (1962) The Bakerian Lecture, 1961: sound generated aerodynamically. Proc R Soc Lon Ser A 267(1329):147–182

Lighthill MJ (1963) Jet noise. AIAA J. 1(7):1507–1517

Lighthill MJ (1978) Waves in fluids. Cambridge University Press

Liu CH, Klostermeyer J, Yeh KC, Jones TB, Robinson T, Holt O et al (1982) Global dynamic responses of the atmosphere to the eruption of Mount St. Helens on May 18, 1980. J Geophys Res Sp Phys 87(A8):6281–6290

Lonzaga JB, Waxler RM, Assink JD, Talmadge CL (2015) Modelling waveforms of infrasound arrivals from impulsive sources using weakly non-linear ray theory. Geophys J Int 200:1347–1361

Lopez T, Fee D, Prata F, Dehn J (2013) Characterization and interpretation of volcanic activity at Karymsky Volcano, Kamchatka, Russia, using observations of infrasound, volcanic emissions, and thermal imagery. Geochem Geophys Geosyst 14(12):5106–5127. https://doi.org/10.1002/2013GC004817

Lorenz RD, Turtle EP, Howell R, Radebaugh J, Lopes RM (2015) The roar of Yasur: Handheld audio recorder monitoring of Vanuatu volcanic vent activity, *J*. Geotherm Res, Volcanol in press

Lyons JJ, Ichihara M, Kurokawa A, Lees JM (2013) Switching between seismic and seismo-acoustic harmonic tremor simulated in the laboratory: insights into the role of open degassing channels and magma viscosity. J Geophys Res Solid Earth 118(1):277–289

Marchetti E, Ichihara M, Ripepe M (2004) Propagation of acoustic waves in a viscoelastic two-phase system: influence of gas bubble concentration. J Volcanol Geotherm Res 137(1–3):93–108. https://doi.org/10.1016/j.jvolgeores.2004.05.002

Marchetti E, Ripepe M, Harris AJL, Delle Donne D (2009) Tracing the differences between Vulcanian and Strombolian explosions using infrasonic and thermal radiation energy. Earth Planet Sci Lett 279(3):273–281

Marchetti E, Ripepe M, Delle Donne D, Genco R, Finizola A, Garaebiti E (2013) Blast waves from violent explosive activity at Yasur Volcano, Vanuatu. Geophys Res Lett 40(22):5838–5843

Marchetti E, Ripepe M, Campus P, Le Pichon A, Brachet N, Blanc E, Gaillard P, Mialle P, Husson P (2019) Infrasound monitoring of volcanic eruptions and contribution of ARISE to the volcanic ash advisory centers. In: Le Pichon A, Blanc E, Hauchecorne A (eds) Infrasound monitoring for atmospheric studies, 2nd edn. Springer, Dordrecht, pp 1141–1162

Marcillo O, Johnson JB (2010) Tracking near-surface atmospheric conditions using an infrasound network. J Acoust Soc Am 128:EL14–19, https://doi.org/10.1121/1.3442725

Matoza RS, Hedlin MSH, Garces MA (2007) An infrasound array study of Mount St. Helens. J Volcanol Geotherm. Res. 160:249–262. https://doi.org/10.1016/j.jvolgeores.2006.10.006

Matoza RS, Garces MA, Chouet BA, D'Auria L, Hedlin MAH, de Groot-Hedlin C, Waite GP (2009a) The source of infrasound associated with long-period events at Mount St. Helens. J Geophys Res 114:B04305. https://doi.org/10.1029/2008jb006128

Matoza RS, Fee D, Garces MA, Seiner JM, Ramon PA, Hedlin MAH (2009b) Infrasonic jet noise from volcanic eruptions. Geophys Res Lett 36:L08303. https://doi.org/10.1029/2008GL036486

Matoza RS, Fee D, Garces M (2010) Infrasonic tremor wavefield of the Pu'u O'o crater complex and lava tube system, Hawaii, in April 2007. J Geophys Res 115:B12312. https://doi.org/10.1029/2009JB007192

Matoza RS, Le Pichon A, Vergoz J, Herry P, Lalande J, Lee H, Che I, Rybin A (2011a) Infrasonic observations of the June 2009 Sarychev Peak eruption, Kuril Islands: implications for infrasonic monitoring of remote explosive volcanism. J Volcanol Geotherm Res 200:35–48. https://doi.org/10.1016/j.jvolgeores.2010.11.022

Matoza RS, Vergoz J, Le Pichon A, Ceranna L, Green DN, Evers LG, Ripepe M, Campus P, Liszka L, Kvaerna T, Kjartansson E, Hoskuldsson A (2011b) Long-range acoustic observations of the Eyjafjallajökull eruption, Iceland, April-May 2010. Geophys Res Lett 38:L06308. https://doi.org/10.1029/2011GL047019

Matoza RS, Shearer PM, Lin G, Wolfe CJ, Okubo PG (2013a) Systematic relocation of seismicity on Hawaii Island from 1992 to 2009 using waveform cross correlation and cluster analysis. J Geophys Res Solid Earth 118(5):2275–2288

Matoza RS, Fee D, Neilsen TB, Gee KL, Ogden DE (2013b) Aeroacoustics of volcanic jets: acoustic power estimation and jet velocity dependence. J Geophys Res Solid Earth 118:6269–6284. https://doi.org/10.1002/2013JB010303

Matoza RS, Landès M, Le Pichon A, Ceranna L, Brown D (2013c) Coherent ambient infrasound recorded by the International Monitoring System. Geophys Res Lett 40. https://doi.org/10.1029/2012gl054329

Matoza RS, Fee D (2014) Infrasonic component of volcano-seismic eruption tremor. Geophys Res Lett 41:2014GL059301. https://doi.org/10.1002/2014gl059301

Matoza RS, Fee D, Lopez TM (2014) Acoustic characterization of explosion complexity at Sakurajima, Karymsky, and Tungurahua Volcanoes. Seismol Res Lett 85(6):1187–1199. https://doi.org/10.1785/0220140110

Matoza RS, Green DN, Le Pichon A, Shearer PM, Fee D, Mialle P, Ceranna L (2017) Automated detection and cataloging of global explosive volcanism using the International Monitoring System infrasound network. J Geophys Res Solid Earth 122:2946–2971. https://doi.org/10.1002/2016JB013356

Mauk FJ (1983) Utilization of seismically recorded infrasonic-acoustic signals to monitor volcanic explosions: the El Chichon Sequence 1982–A case study. J Geophys Res Solid Earth 88 (B12):10385–10401

Mialle P et al (2015) Towards a volcanic notification system with infrasound data: use of infrasound data in support of the VAACs in the framework of ARISE project. In: World meteorological organization 7th international workshop on volcanic ash (IWVA/7), Anchorage, Alaska

McNutt SR (2000) Seismic monitoring. In: Sigurdsson H (ed) Encyclopedia of volcanoes. Academic Press, San Diego, Calif

McNutt SR, Nishimura T (2008) Volcanic tremor during eruptions: temporal characteristics, scaling and constraints on conduit size and processes. J Volcanol Geotherm Res 178:10–18. https://doi.org/10.1016/j.jvolgeores.2008.03.010

McNutt SR, Thompson G, Johnson J, De Angelis S, Fee D (2015) Seismic and infrasonic monitoring, Chapter 63. In: Sigurdsson H, Houghton B, McNutt S, Rymer H (eds) The Encyclopedia of Volcanoes, Second Edition. Academic Press, J. Stix, pp 1071–1099

Medici EF, Allen JS, Waite GP (2014) Modeling shock waves generated by explosive volcanic eruptions. Geophys Res Lett 41(2):414–421

Moran SC, Matoza RS, Garces MA, Hedlin MAH, Bowers D, Scott WE, Sherrod DR, Vallance JW (2008) Seismic and acoustic recordings of an unusually large rockfall at Mount St. Helens, Washington. Geophys Res Lett 35(19). https://doi.org/10.1029/2008gl035176
Morrissey MM, Chouet BA (1997) Burst conditions of explosive volcanic eruptions recorded on microbarographs. Science 275(5304):1290–1293
Morse PM, Ingard KU (1968) Theoretical acoustics. McGraw-Hill, Princeton, NJ
Needham CE (2010) Blast wave propagation. Springer, Berlin, Germany, pp 87–99
Newhall CG, Self S (1982) The volcanic explosivity index (VEI): an estimate of explosive magnitude of historical volcanism. J Geophys Res 87:1231–1238
Nishida K, Ichihara M (2016) Real-time infrasonic monitoring of the eruption at a remote island volcano using seismoacoustic cross correlation. Geophys J Int 204(2):748–752
Omori F (1912) The eruptions and earthquakes of the Asama-Yama. Bull Imp Earthq Inv Commitee 6(1)
Oshima H, Maekawa T (2001) Excitation process of infrasonic waves associated with Merapi-type pyroclastic flow as revealed by a new recording system. Geophys Res Lett 28(6):1099–1102
Ostashev VE (1997) Acoustics in moving inhomogeneous media. E & FN Spon, London
Pekeris CL (1939) The propagation of a pulse in the atmosphere. Proc R Soc LonSer A 171 (947):434–449
Perret FA (1950) Volcanological Observations. Carnegie Institution Of Washington Publication
Pierce AD (1963) Propagation of acoustic-gravity waves from a small source above the ground in an isothermal atmosphere. J Acoust Soc Am 35(11):1798–1807
Pierce AD (1989) Acoustics: an introduction to its physical principals and applications. Acoustical Society of America, Melville, N. Y.
Piercy JE, Embleton TFW, Sutherland LC (1977) Review of noise propagation in the atmosphere. J Acoust Soc Am 61(6):1403–1418
Prejean SG, Brodksy EE (2011) Volcanic plume height measured by seismic waves based on a mechanical model. J Geophys Res 116:B01306. https://doi.org/10.1029/2010JB007620
Press F, Harkrider D (1962) Propagation of acoustic-gravity waves in the atmosphere. J Geophys Res 67(10):3889–3908
Press F, Harkrider D (1966) Air-sea waves from the explosion of Krakatoa. Science 154 (3754):1325–1327
Reed JW (1977) Atmospheric attenuation of explosion waves. J Acoust Soc Am 61(1):39–47
Reed JW (1987) Air-pressure waves from Mount St. Helens Eruptions. J Geophys Res Atmos 92 (D10):11979–11992, https://doi.org/10.1029/jd092id10p11979
Reynolds JWS (1878) The theory of sound, vol II. The Macmillan Company
Richards AF (1963) Volcanic sounds, investigation and analysis. J Geophys Res Solid Earth 68:919–928
Richardson JP, Waite GP, Palma JL (2014) Varying seismic-acoustic properties of the fluctuating lava lake at Villarrica volcano, Chile. J Geophys Res Solid Earth 119(7):5560–5573
Ripepe M, Poggi P, Braun T, Gordeev E (1996) Infrasonic waves and volcanic tremor at Stromboli. Geophys Res Lett 23(2):181–184
Ripepe M, Marchetti E (2002) Array tracking of infrasonic sources at Stromboli volcano. Geophys Res Lett 29(22)
Ripepe M, Marchetti E (2019) Infrasound monitoring of volcano-related hazards for civil protection. In: Le Pichon A, Blanc E, Hauchecorne A (eds) Infrasound monitoring for atmospheric studies, 2nd edn. Springer, Dordrecht, pp 1107–1140
Ripepe M, Marchetti E, Ulivieri G (2007) Infrasonic monitoring at Stromboli volcano during the 2003. J Geophys Res Solid Earth 112:B09207. https://doi.org/10.1029/2006JB004613
Ripepe M, De Angelis S, Lacanna G, Poggi P, Williams C, Marchetti E, Donne DD, Ulivieri G. Tracking pyroclastic flows at Soufrière Hills Volcano (2009) Eos. Trans Am GeophysChile 90 (27):229–30
Ripepe M, De Angelis S, Lacanna G, Voight B (2010a) Observation of infrasonic and gravity waves at Soufrière Hills Volcano, Montserrat. Geophys Res Lett. 37(L00E14). https://doi.org/10.1029/2010gl042557

Ripepe M, Marchetti E, Bonadonna C, Harris AJL, Pioli L, Ulivieri G (2010b) Monochromatic infrasonic tremor driven by persistent degassing and convection at Villarrica Volcano, Chile. Geophys Res Lett 37:L15303. https://doi.org/10.1029/2010gl043516

Ripepe M, Bonadonna C, Folch A, Delle Donne D, Lacanna G, Marchetti E, Höskuldsson A (2013) Ash-plume dynamics and eruption source parameters by infrasound and thermal imagery: the 2010 Eyjafjallajökull eruption. Earth Planet Sci Lett 366:112–121

Rowell CR, Fee D, Szuberla CAL, Arnoult K, Matoza RS, Firstov PP, Kim K, Makhmudov E (2014) Three-dimensional volcano-acoustic source localization at Karymsky Volcano, Kamtchatka, Russia. J Volcanol Geotherm Res 283:101–115. https://doi.org/10.1016/j.volgeores.2014.06.015

Sahetapy-Engel ST, Harris AJ, Marchetti E (2008) Thermal, seismic and infrasound observations of persistent explosive activity and conduit dynamics at Santiaguito lava dome, Guatemala. J Volcanol Geoth Res 173(1):1–14

Sakai T, Yamasato H, Uhira K (1996) Infrasound accompanying C-type tremor at Sakurajima volcano. Bull Volcano Soc Jpn 41:181–185 (in Japanese)

Scott RH (1884) Note on a series of barometrical disturbances which passed over Europe between the 27th and the 31st of August, 1883. Proc R Soc Lon 36:139–143

Segall P (2010) Earthquake and volcano deformation. Princeton University Press, New Jersey

Siebert L, Simkin T (2002-) Volcanoes of the world: an illustrated catalog of Holocene volcanoes and their eruptions, Smithsonian Institution, Global Volcanism Program digital information series, GVP-3

Snodgrass JM, Richards AF (1956) Observations of underwater volcanic acoustics at Barcena volcano, San Benedicto Island, Mexico, and in Shelikof Strait, Alaska. Trans Am Geophys Union 37:97–104

Sparks, RSJ, Burski MI, Carey SN, Gilbert JS, Glaze LS, Sigurdsson H, Woods AW (1997) Volcanic plumes. Wiley-Blackwell

Strachey RH (1884) Note on the foregoing paper. Proc R Soc Lond 36:143–151

Strachey RH (1888) On the air waves and sounds caused by the eruption of Krakatoa in August 1883. In: Symons GJ (ed) The eruption of Krakatoa and subsequent phenomena, Report of the Krakatoa Committee of the Royal Society, Trübner and Co, Ludgate Hill

Sutherland LC, Bass HE (2004) Atmospheric absorption in the atmosphere up to 160 km. J Acoust Soc Am 115(3):1012–1032. https://doi.org/10.1121/1.1631937

Taddeucci J, Scarlato P, Capponi A, Del Bello E, Cimarelli C, Palladino DM, Kueppers U (2012) High-speed imaging of Strombolian explosions: the ejection velocity of pyroclasts. Geophys Res Lett 39:L02301. https://doi.org/10.1029/2011GL050404

Taddeucci J, Sesterhenn J, Scarlato P, Stampka K, Del Bello E, Pena Fernandez JJ, Gaudin D (2014) High-speed imaging, acoustic features, and aeroacoustic computations of jet noise from Strombolian (and Vulcanian) explosions. Geophys Res Lett 41(9):2014GL059925. https://doi.org/10.1002/2014gl059925

Tahira M (1982) A study of the infrasonic wave in the atmosphere: (II) infrasonic waves generated by the explosions of the volcano Sakurajima. J Meteorol Soc Jpn 60(3):896–907

Tahira M, Nomura M, Sawada Y, Kamo K (1996) Infrasonic and acoustic-gravity waves generated by the Mount Pinatubo eruption of June 15, 1991. In: Newhall C, Punongbayan R (eds) Fire and mud: eruptions and lahars of mount Pinatubo, Philippines. University of Washington Press, Seattle and London

Tailpied D, Le Pichon A, Marchetti E, Ripepe M, Kallel M, Ceranna L, Brachet N (2013) Remote infrasound monitoring of Mount Etna: observed and predicted network detection capability. InfraMatics 2(1). https://doi.org/10.4236/inframatics.2013.21001

Taisne B, Whelley P, Le Pichon A, Newhall C (2012) On the use of an infrasonic array at Singapore for volcanoes monitoring, EGU General Assembly

Taisne B, Perttu A, Tailpied D, Caudron C, Simonini L (2019) Atmospheric controls on ground- and space-based remote detection of volcanic ash injection into the atmosphere, and link to early warning systems for aviation hazard mitigation. In: Le Pichon A, Blanc E,

Hauchecorne A (eds) Infrasound monitoring for atmospheric studies, 2nd edn. Springer, Dordrecht, pp 1079–1105
Tam CKW (1998) Jet noise: since 1952. Theor Comput Fluid Dyn 10:393–405
Tam CKW, Viswanathan K, Ahuja KK, Panda J (2008) The sources of jet noise: experimental evidence. J Fluid Mech 615:253–292
Taylor GI (1929) Waves and tides in the atmosphere. Proc R Soc Lond Ser A, 126(800):169–183
Taylor GI (1936) The oscillations of the atmosphere. Proc R Soc Lond Ser A, 156(888):318–326
Tempest A, Flett JS (1903) Report on the Eruptions of the Soufriere, in St. Vincent, in 1902, and on a Visit to Montagne Pelee, in Martinique - Part I. Philos Trans R Soc Lond Ser A 200: 353–553
Tupper A, Itikarai I, Richards M, Prata F, Carn S, Rosenfeld D (2007) Facing the challenges of the international airways volcano watch: the 2004/05 eruptions of Manam, Papua New Guinea. Weather Forecast 22(1):175–191
Ulivieri G, Ripepe M, Marchetti E (2013) Infrasound reveals transition to oscillatory discharge regime during lava fountaining: implication for early warning. Geophys Res Lett 40(12): 3008–3013
Verbeek (1884) The Krakatoa eruption. Nature 30(757):10–15
Vergniolle S, Brandeis G (1994) Origin of the sound generated by strombolian explosions. Geophys Res Lett 21:1959–1962
Vergniolle S, Brandeis G, Mareschal JC (1996) Strombolian explosions: 2. Eruption dynamics determined from acoustic measurements. J Geophys Res Solid Earth 101(B9):20449–20466
Vergniolle S, Caplan-Auerbach J (2006) Basaltic thermals and subplinian plumes: constraints from acoustic measurements at Shishaldin volcano, Alaska. Bull Volcanol 68(7–8):611–630
Vidal V, Ripepe M, Divoux T, Legrand D, Géminard JC, Melo F (2010) Dynamics of soap bubble bursting and its implications to volcano acoustics. Geophys Res Lett 37(7)
Viswanathan K (2009) Mechanisms of jet noise generation: classical theories and recent developments. Int J Aeroacoust 8(4):355–408
Walker KT, Hedlin MAH (2010) A review of wind-noise reduction methodologies. In: Pichon AL, Blanc E, Hauchecorne A (eds) Infrasound monitoring for atmospheric studies, chap. 5, Springer, Netherlands, pp 141–182
Watada S, Kanamori H (2010) Acoustic resonant oscillations between the atmosphere and the solid earth during the 1991 Mt. Pinatubo eruption. J Geophys Res Solid Earth 115:B12319. https://doi.org/10.1029/2010JB007747
Waythomas CF, Haney MM, Fee D, Schneider DJ, Wech A (2014) The 2013 eruption of Pavlof Volcano, Alaska: a spatter eruption at an ice-and snow-clad volcano. Bull Volcanol 76(10): 1–12
Wilson CR, Forbes RB (1969) Infrasonic waves from Alaskan volcanic eruptions. J Geophys Res 74:4511–4522
Wilson CR, Nichparenko S, Forbes RB (1966) Evidence of two sound channels in the polar atmosphere from infrasonic observations of the eruption of an Alaskan volcano. Nature 211:163–165
Woulff G, McGetchin TR (1976) Acoustic noise from volcanoes: theory and experiment. Geophys J R Astr Soc 45:601–616
Yamasato H (1997) Quantitative analysis of pyroclastic flows using infrasonic and seismic data at Unzen volcano, Japan. J Phys Earth 45(6):397–416
Yamasato H (1998) Nature of infrasonic pulse accompanying low frequency earthquake at Unzen Volcano, Japan. Bull Volcanol Soc Jpn 43:1–13
Yokoo A, Ishihara K (2007) Analysis of pressure waves observed in Sakurajima eruption movies. Earth Planet Sp 59(3):177–181
Yokoo A, Tameguri T (2007) Iguchi M (2009) Swelling of a lava plug associated with a Vulcanian eruption at Sakurajima Volcano, Japan, as revealed by infrasound record: case study of the eruption on January 2. Bull Volc 71(6):619–630. https://doi.org/10.1007/s00445-008-0247-5
Yokoo A, Iguchi M, Tameguri T, Yamamoto K (2013) Processes prior to outbursts of vulcanian eruption at Showa crater of Sakurajima volcano. Bull Volcanol Soc Jpn 58:163–181